

# Folding Cooperativity of Synthetic Polypeptides with or without “Tertiary” Interactions

Yuan Ren<sup>[a]</sup>, Hailin Fu<sup>[a]</sup>, Ryan Baumgartner<sup>[c]</sup>, Yanfeng Zhang<sup>[d]</sup>, Jianjun Cheng <sup>[c,d]\*</sup>,  
Yao Lin <sup>[a,b]\*</sup>

[a]Department of Chemistry, [b]Polymer Program, Institute of Material Science,  
University of Connecticut, Storrs, CT, USA;

[c]Department of Chemistry, [d]Department of Materials Science and Engineering,  
University of Illinois at Urbana-Champaign, Urbana, IL, USA;

\* To whom the correspondences should be addressed.

## Table of Contents

Synthesis and characterization of polymers.....	2
TFA/Temperature induced helix-coil transitions studies for PZLL containing polymers.....	5
Model-based analysis of TFA- and temperature-induced helix-coil transitions of linear PZLLs. ....	32
NOESY study of PZLL containing polymers. ....	33
Effect of variation of $\sigma$ on the fitting of PZLL-grafted comb macromolecules. ....	37
Effect of variation of chain length (N) on the fitting of PZLL-grafted comb macromolecules. ....	38

**General Experimental Considerations:** All reagents and solvents were purchased from Sigma-Aldrich and used as received unless otherwise specified. All polymerizations were mixed in an MBraun glovebox under argon. Dry solvents were prepared by passing nitrogen purged solvents through activated alumina columns. All dry solvents were stored over 4Å sieves in the glovebox.  $\epsilon$ -Cbz-*L*-lysine NCA was synthesized according to previous methods.<sup>1</sup>

**Instrumentation:** Nuclear magnetic resonance (NMR) spectra were recorded on a Bruker DRX 500 MHz spectrometer for polymer characterization. Chemical shifts are referenced to residual protons in the deuterated NMR solvents. MestReNova 8.1.1 was used to analyze all spectra. Fourier transform infrared (IR) spectra were performed using a Spectrum 100 spectrometer (Perkin Elmer). Gel Permeation Chromatography (GPC) was performed on a system equipped with a Model 1200 isocratic pump (Agilent Technology) in series with a 717 Autosampler (Waters) and size exclusion columns (10<sup>2</sup> Å, 10<sup>3</sup> Å, 10<sup>4</sup> Å, 10<sup>5</sup> Å, 10<sup>6</sup> Å Phenogel columns, 5 µm, 300 × 7.8 mm, Phenomenex) which were maintained at a temperature of 60°C. A DAWN HELEOS (Wyatt Technology) multiangle laser light scattering (MALLS) operating at a wavelength of 658 nm and an Optilab rEX refractive index detector (Wyatt Technology) operating at a wavelength of 658 nm were used as detectors. The mobile phase consisted of *N,N*-dimethylformamide (DMF) containing 0.1M LiBr at a flow rate of 1 mL min<sup>-1</sup>. Samples were filtered through a 0.45 µm PTFE filter before analysis. Absolute molecular weights of polymers were determined using ASTRA 6.1.1.17 software (Wyatt Technology) and calculated from  $dn/dc$  values assuming 100% mass recovery. Polymers for NOESY experiments were dissolved in 99:1 (v:v) CDCl<sub>3</sub>:TFA-*d* and sealed in NMR tubes to prevent solvent evaporation. 2D NOESY experiments were performed on a Bruker DRX-500 MHz spectrometer with the  $(\pi/2)$ - $t_1$ - $(\pi/2)$ - $\tau_m$ - $(\pi/2)$ - $t_2$  pulse sequence. Spectra were acquired with  $t_1$  at 0.15 ms. The  $\pi/2$  pulse width was 8.4 µs,  $\tau_m$  was 100 ms and the delay between acquisitions was 2 s.

**Synthesis of PZLL.** Linear PZLLs were synthesized according to previous methods via the controlled NCA polymerization mediated by *N*-trimethylsilyl allylamine.<sup>2,3</sup>  $\epsilon$ -Cbz-*L*-lysine NCA (Lys-NCA) was dissolved in DMF. The Lys-NCA solution was then added to a DMF solution containing *N*-trimethylsilyl allylamine. The reaction mixture was stirred for 24 h at room temperature. After Lys-NCA was completely consumed (monitored by checking the NCA anhydride stretch at 1790cm<sup>-1</sup> using FT-IR), PZLL was precipitated with methanol and analyzed by GPC. The  $M_n$ ,  $M_w$  and MWD ( $M_w/M_n$ ) were determined by GPC. <sup>1</sup>H NMR (CDCl<sub>3</sub>, 500 MHz):  $\delta$  8.0 (CH-NH-), 7.39-7.25 (ArH-), 6.10 (C<sub>6</sub>H<sub>5</sub>CH<sub>2</sub>-), 3.95 (CH-NH-,  $\alpha$ H-), 3.10 (NH-CH<sub>2</sub>-CH<sub>2</sub>-), 2.90-1.10 (-CH<sub>2</sub>-,  $\beta$ ,  $\gamma$ H-).

**Synthesis of PN-g-PZLL.** PN-g-PZLL brush polymers were synthesized by following the procedure as described before.<sup>2,3</sup> Poly(norbornene-*endo*-2,3-dicarboximide) (PN) bearing *N*-TMS groups was prepared through ROMP in THF or dichloromethane. After removal of the solvent under vacuum, the PN polymers were used to initiate the Lys-NCA polymerization in DMF without further purification. <sup>1</sup>H NMR (CDCl<sub>3</sub>, 500 MHz) for PN-g-PZLL ( $\delta$  8.0, 7.39-7.25, 6.10, 3.95, 3.10, 2.90-1.10).

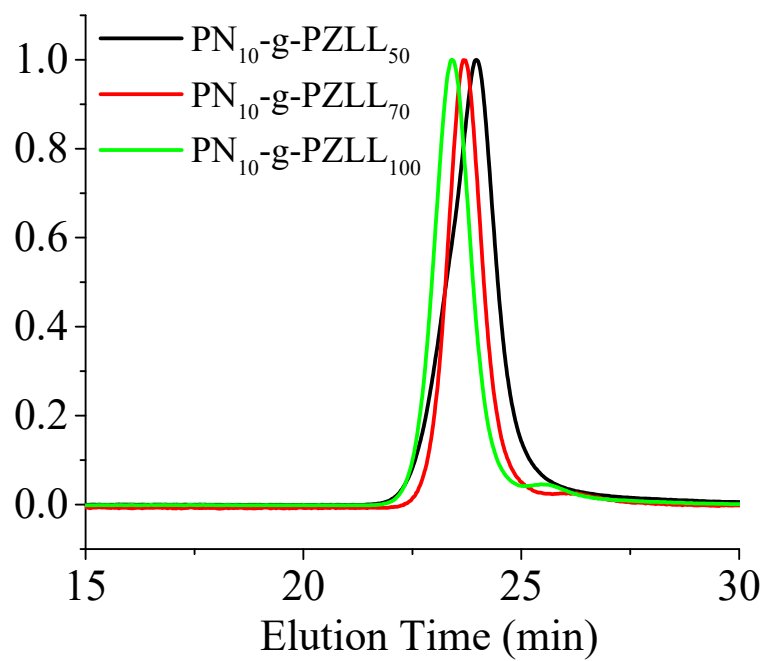


**Figure S1.** Overlay of the normalized GPC-LS traces of PN<sub>10</sub>-g-PZLL<sub>n</sub> (n=50, 70 and 100)

**TFA/Temperature induced helix-coil transitions studies for PZLL containing polymers. (Figure S1-S44).** Solvent and temperature induced helix-coil transition studies were carried out on a Bruker DRX 500 MHzs spectrometer. To prevent the potential aggregation of PZLL chains, at least 1 % TFA-d has been added into the solution. Methods of Goodman and Marborough were applied to study TFA/Temperature induced helix-coil transition of PZLLs. For TFA induced helix-coil transition studies, PZLL containing macromolecules at different solvent compositions were studied at 300 K. While for temperature induced helix-coil transition, PZLL containing macromolecules at predetermined solvent compositions were measured at different temperatures. All the temperature calibrations were performed by measuring the OH resonances and CH<sub>n</sub> resonances in either Methanol or Ethylene glycol. The chemical shifts at 4.0 ppm and 4.6 ppm are used to identify the  $\alpha$ -helix and random coil structures, respectively, accordingly to the methods of Goodman and Marborough. The fractional helicity was calculated from comparing the  $\alpha$ -CH that exists in helical form with the total  $\alpha$ -CH that exists in either helical or coil form. On increasing the volume fraction of TFA in CDCl<sub>3</sub>/TFA-d or decreasing the temperature of the solution, the  $\alpha$ -helix conformation in homo-PZLLs diminishes and eventually disappears, as can be seen from the reduced intensity of  $\alpha$ -CH peak at 4.0 ppm. The TFA/Temperature induced helix-coil transitions are more apparent when plotting the helical contents of PZLLs as a function of TFA volume fraction and temperature.

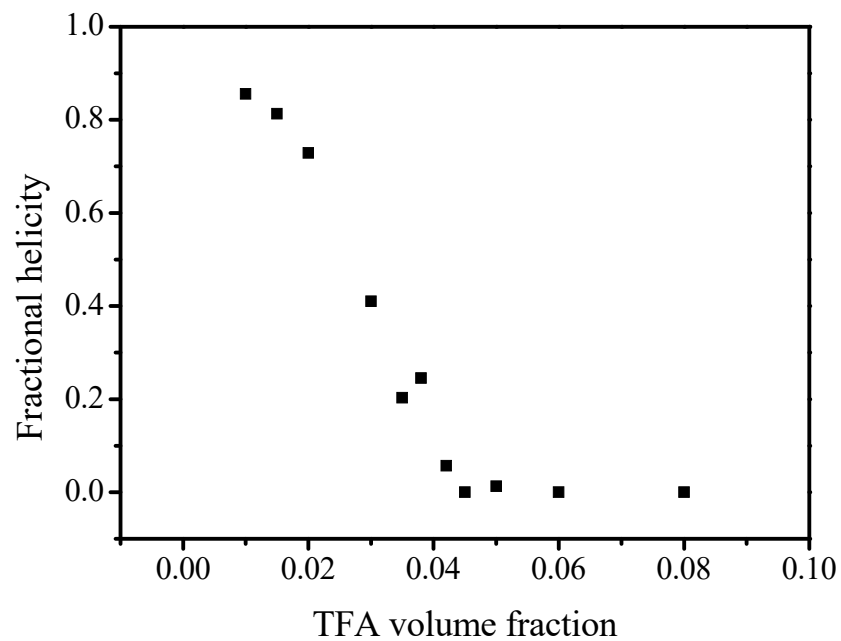
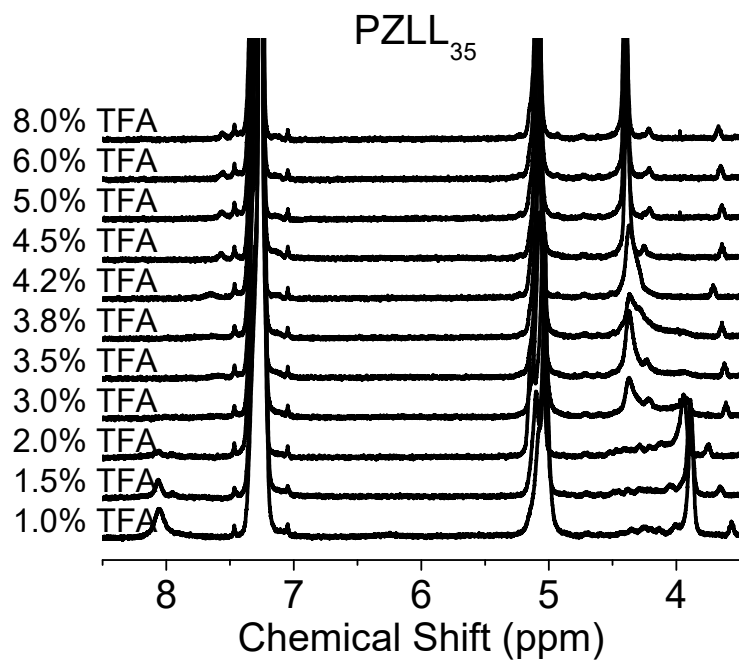


**Figure S2** <sup>1</sup>H NMR spectra of TFA induced helix-to-coil transition of PZLL<sub>35</sub> in TFA-d/CDCl<sub>3</sub> mixture.

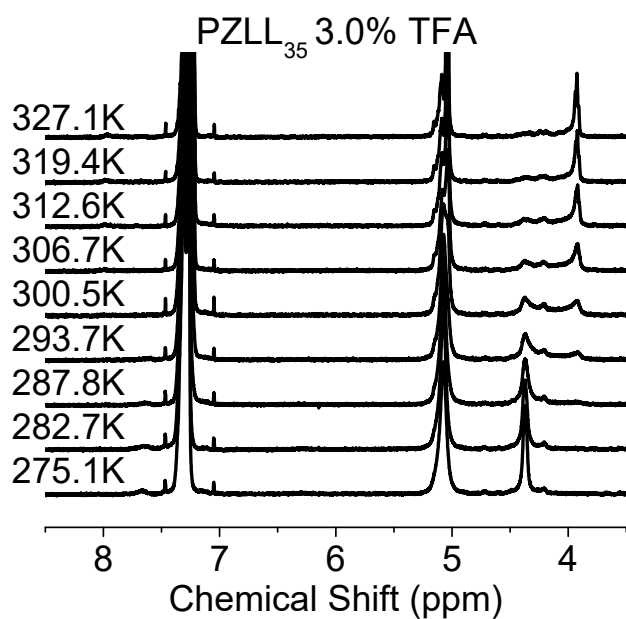


**Figure S3** <sup>1</sup>H NMR spectra of Temperature induced helix-to-coil transition of PZLL<sub>35</sub> in TFA-d/CDCl<sub>3</sub> mixture. The TFA volume concentration is 3.0%

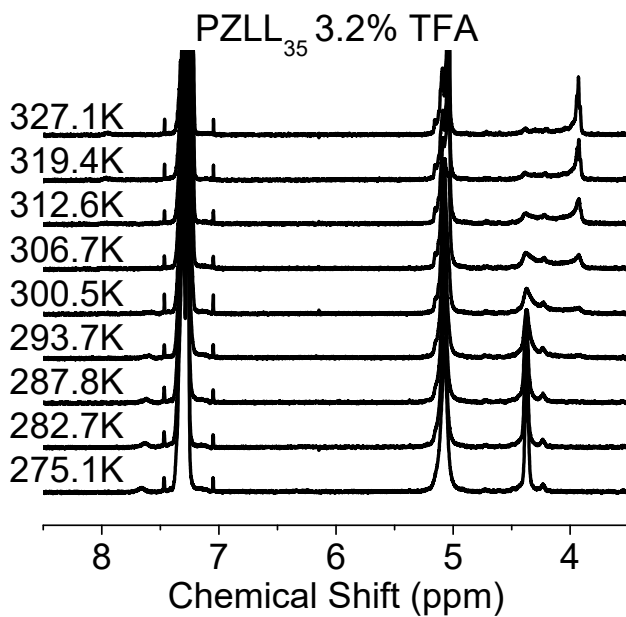


**Figure S4** <sup>1</sup>H NMR spectra of Temperature induced helix-to-coil transition of PZLL<sub>35</sub> in TFA-d/CDCl<sub>3</sub> mixture. The TFA volume concentration is 3.2%

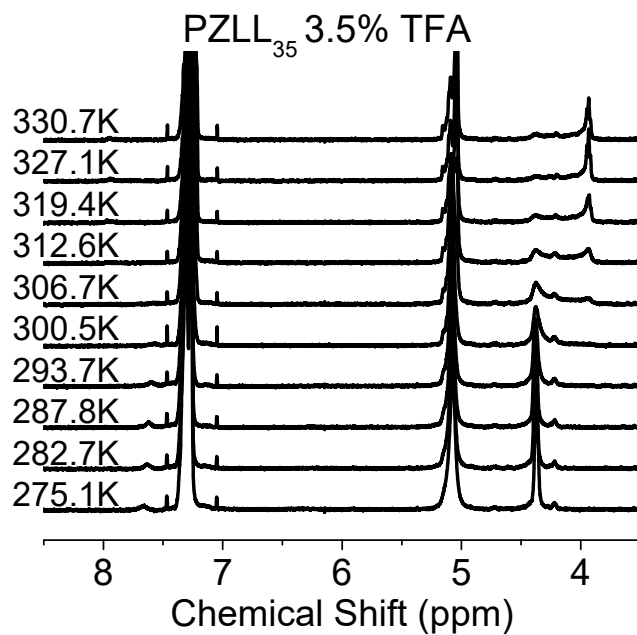


**Figure S5** <sup>1</sup>H NMR spectra of Temperature induced helix-to-coil transition of PZLL<sub>35</sub> in TFA-d/CDCl<sub>3</sub> mixture. The TFA volume concentration is 3.5%

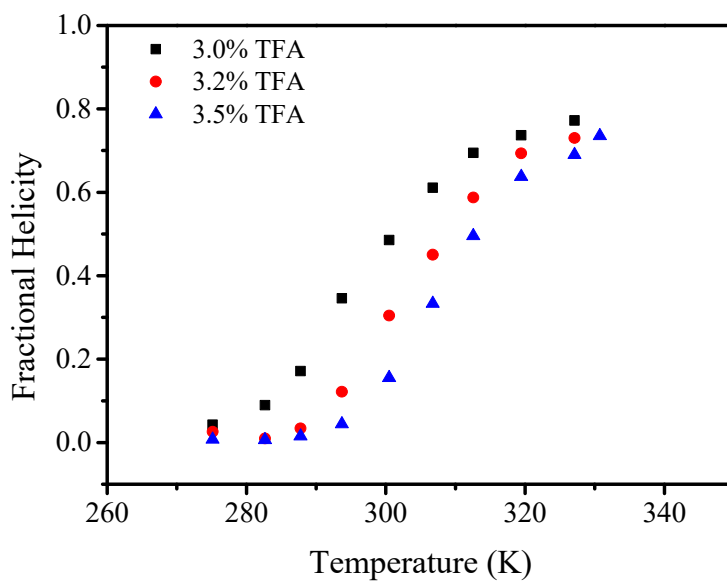


**Figure S6** Temperature induced helix-to-coil transition of PZLL<sub>35</sub> in TFA-d/CDCl<sub>3</sub> mixture.

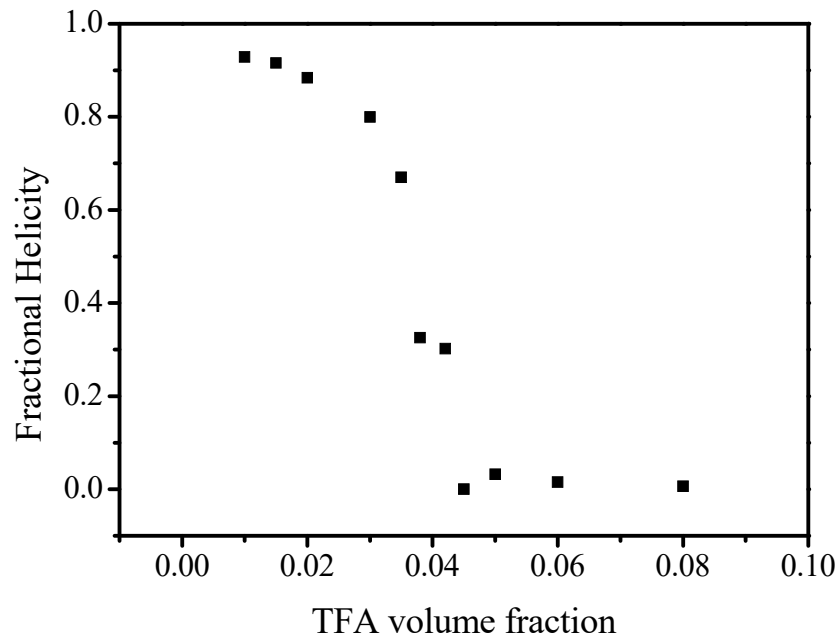
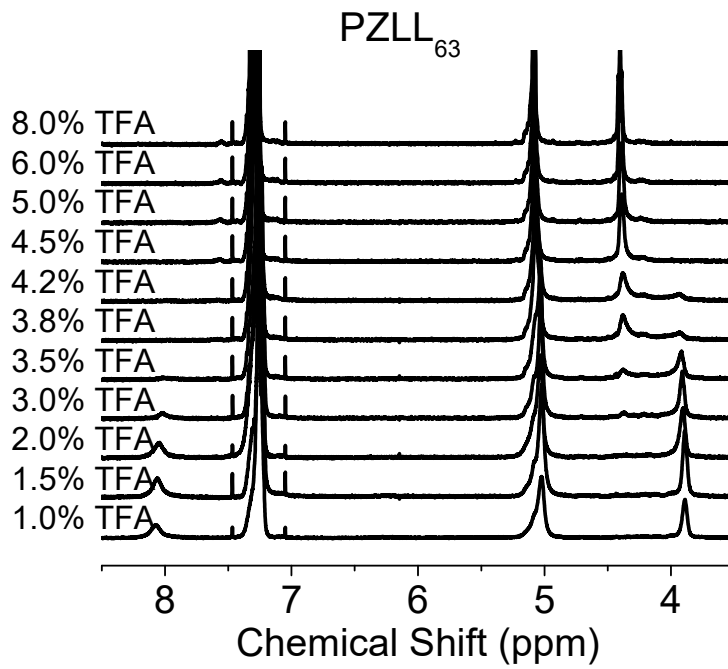


**Figure S7** <sup>1</sup>H NMR spectra of TFA induced helix-to-coil transition of PZLL<sub>63</sub> in TFA-d/CDCl<sub>3</sub> mixture.

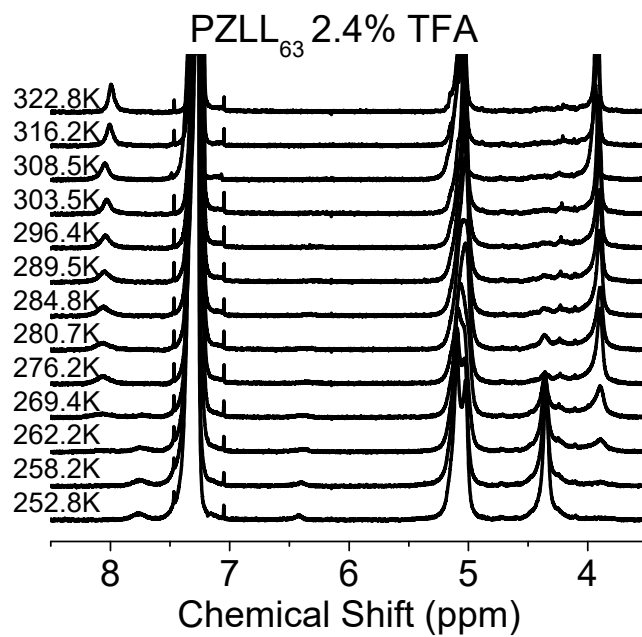


**Figure S8** <sup>1</sup>H NMR spectra of Temperature induced helix-to-coil transition of PZLL<sub>63</sub> in TFA-d/CDCl<sub>3</sub> mixture. The TFA volume concentration is 2.4%

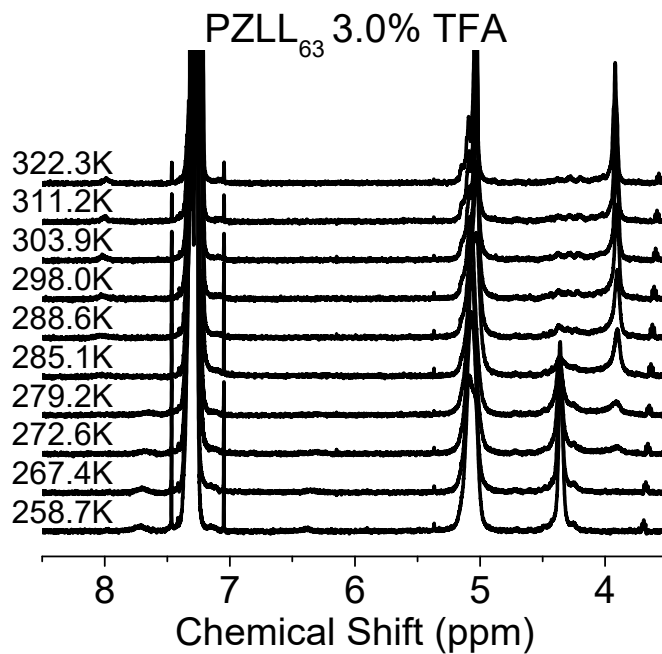


**Figure S9** <sup>1</sup>H NMR spectra of Temperature induced helix-to-coil transition of PZLL<sub>63</sub> in TFA-d/CDCl<sub>3</sub> mixture. The TFA volume concentration is 3.0%

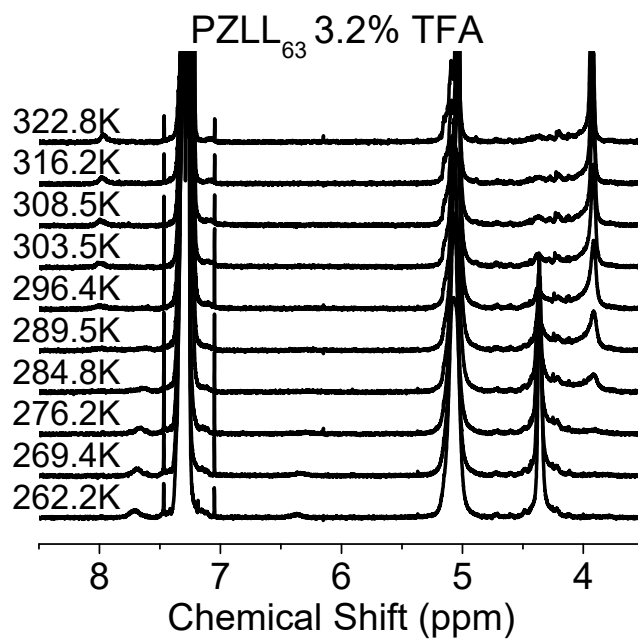


**Figure S10** <sup>1</sup>H NMR spectra of Temperature induced helix-to-coil transition of PZLL<sub>63</sub> in TFA-d/CDCl<sub>3</sub> mixture. The TFA volume concentration is 3.2%

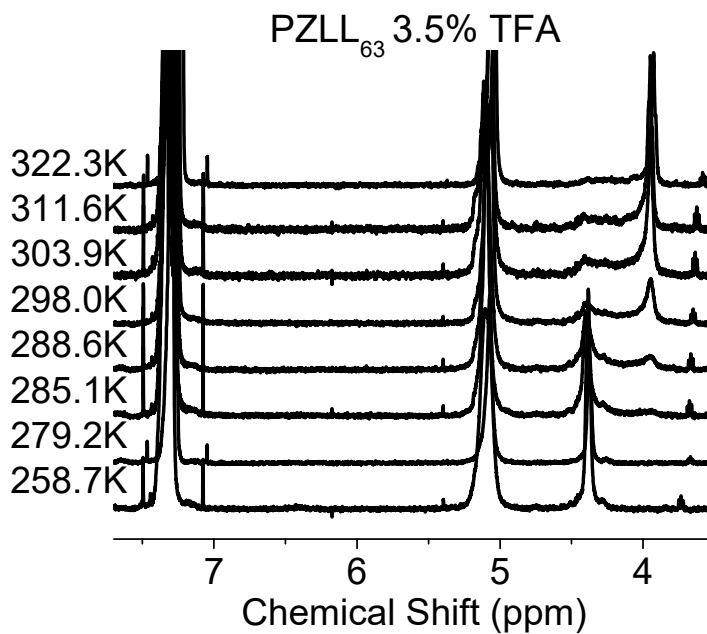


**Figure S11** <sup>1</sup>H NMR spectra of Temperature induced helix-to-coil transition of PZLL<sub>63</sub> in TFA-d/CDCl<sub>3</sub> mixture. The TFA volume concentration is 3.5%

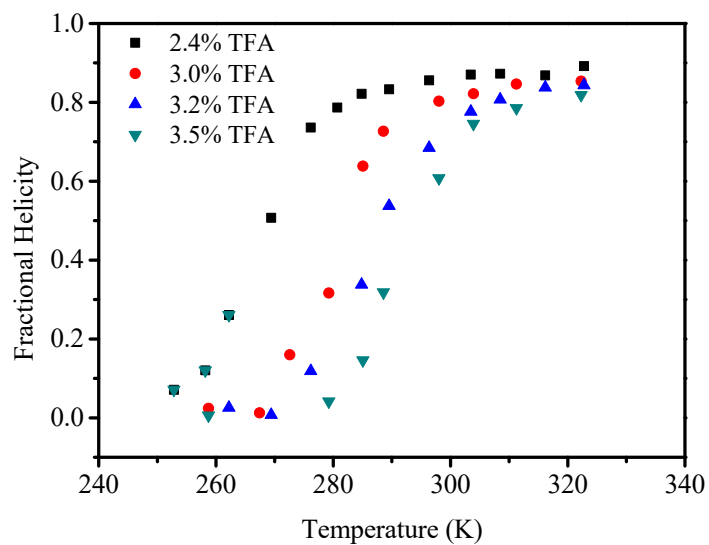


**Figure S12** Temperature induced helix-to-coil transition of PZLL<sub>63</sub> in TFA-d/CDCl<sub>3</sub> mixture.

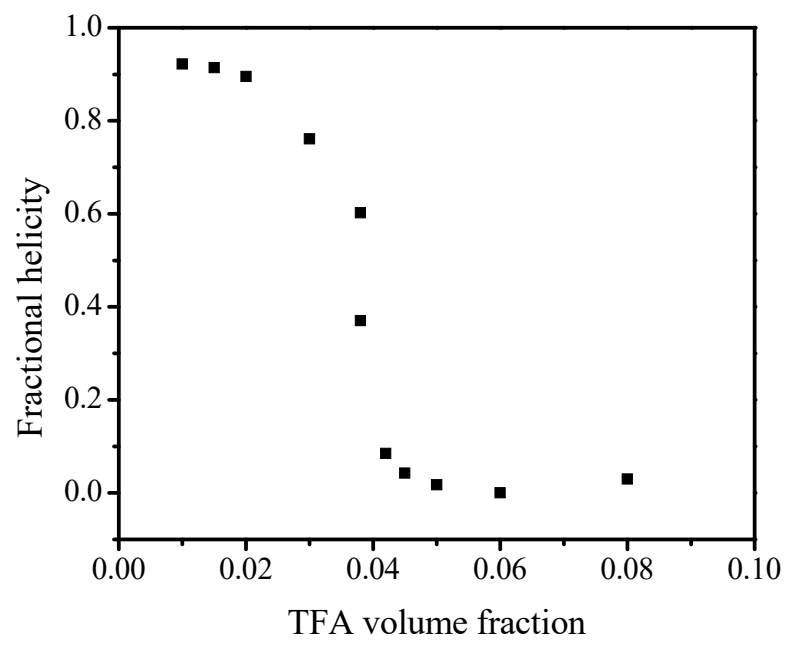
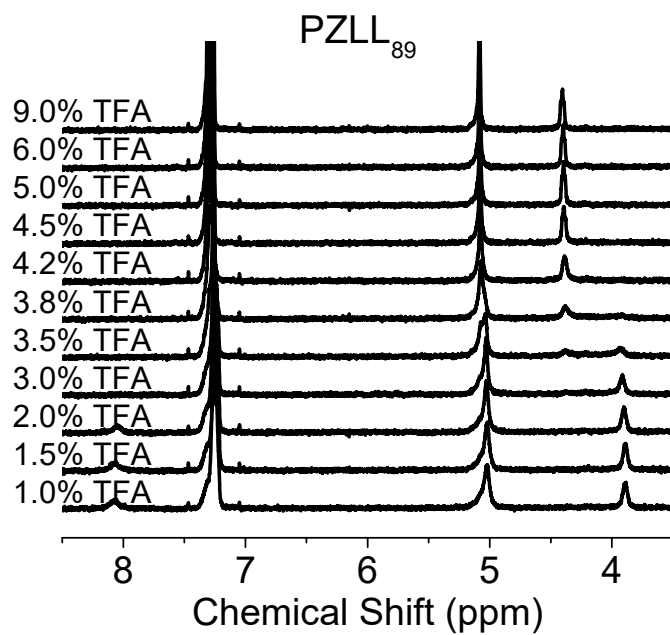


**Figure S13** <sup>1</sup>H NMR spectra of TFA induced helix-to-coil transition of PZLL<sub>89</sub> in TFA-d/CDCl<sub>3</sub> mixture.

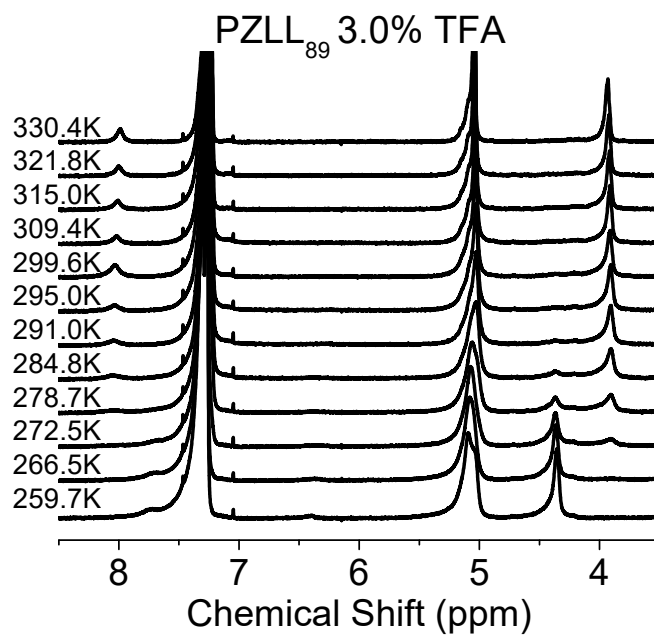


**Figure S14** <sup>1</sup>H NMR spectra of Temperature induced helix-to-coil transition of PZLL<sub>89</sub> in TFA-d/CDCl<sub>3</sub> mixture. The TFA volume concentration is 3.0%

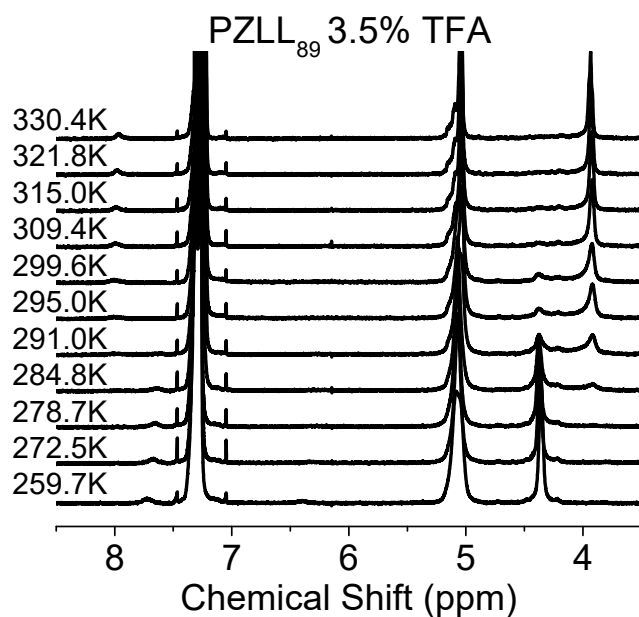


**Figure S15** <sup>1</sup>H NMR spectra of Temperature induced helix-to-coil transition of PZLL<sub>89</sub> in TFA-d/CDCl<sub>3</sub> mixture. The TFA volume concentration is 3.5%

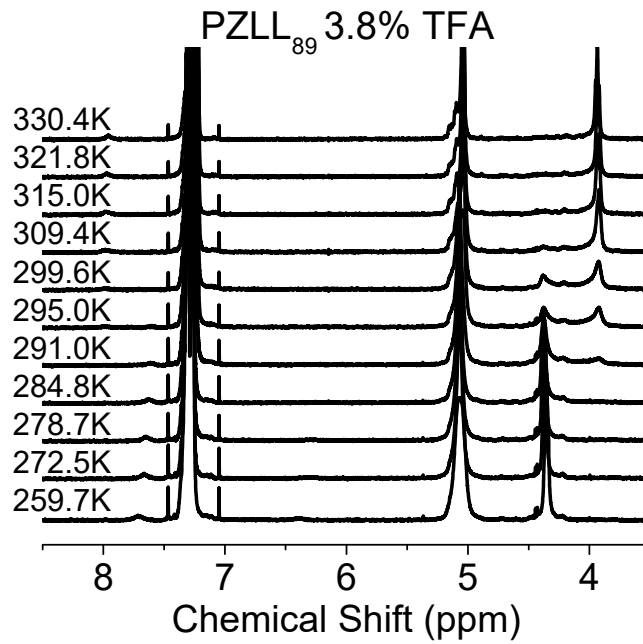


**Figure S16** <sup>1</sup>H NMR spectra of Temperature induced helix-to-coil transition of PZLL<sub>89</sub> in TFA-d/CDCl<sub>3</sub> mixture. The TFA volume concentration is 3.8%

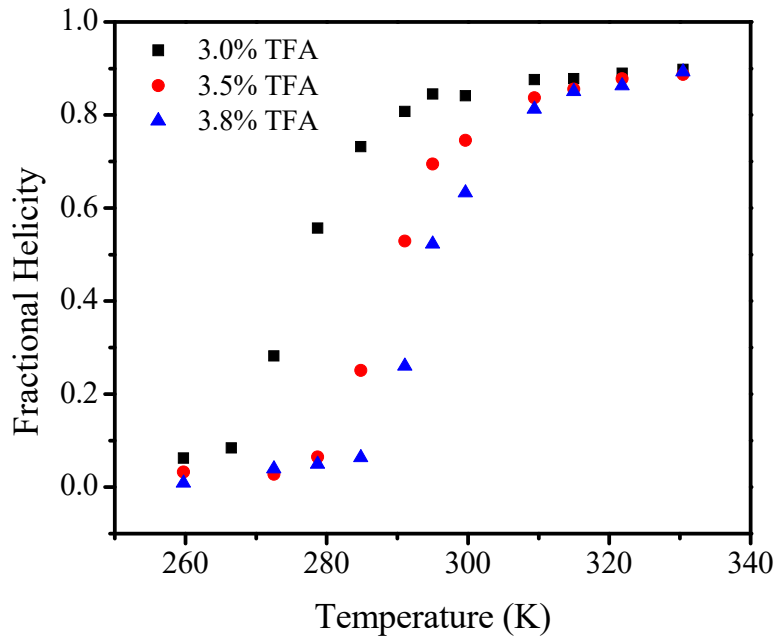


**Figure S17** Temperature induced helix-to-coil transition of PZLL<sub>89</sub> in TFA-d/CDCl<sub>3</sub> mixture.

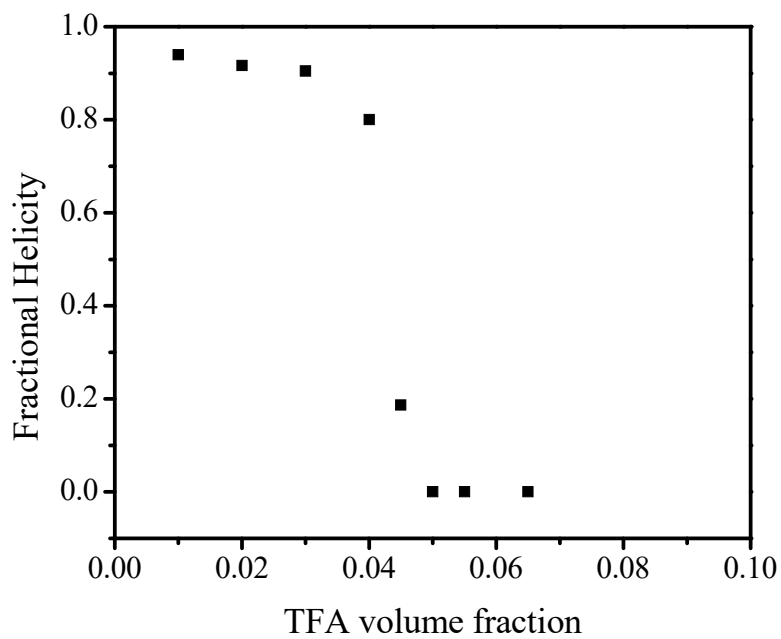
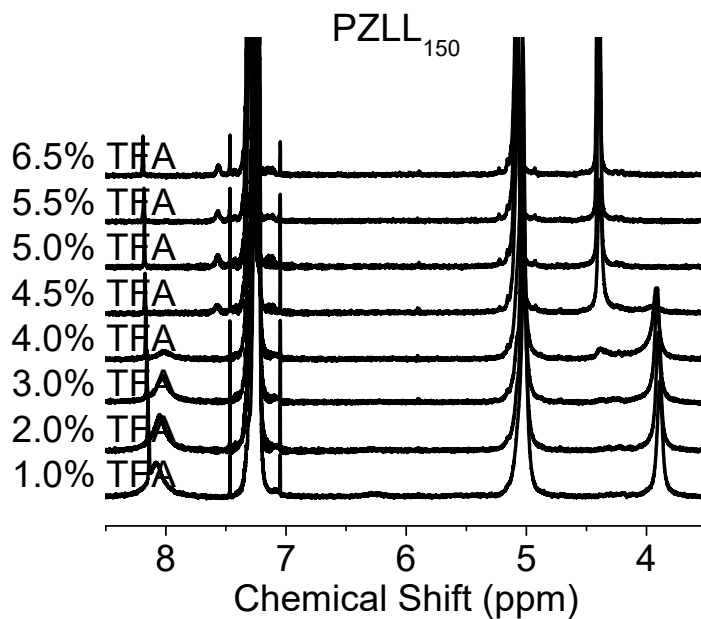


**Figure S18** <sup>1</sup>H NMR spectra of TFA induced helix-to-coil transition of PZLL<sub>150</sub> in TFA-d/CDCl<sub>3</sub> mixture.

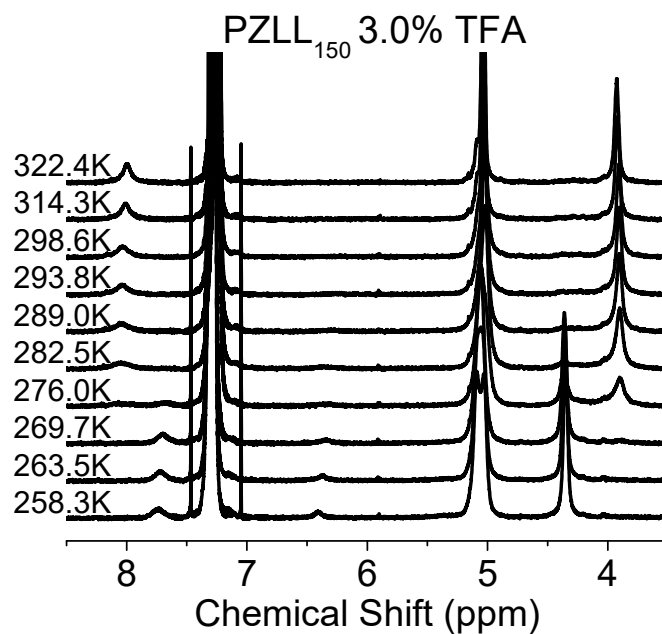


**Figure S19** <sup>1</sup>H NMR spectra of Temperature induced helix-to-coil transition of PZLL<sub>150</sub> in TFA-d/CDCl<sub>3</sub> mixture. The TFA volume concentration is 3.0%

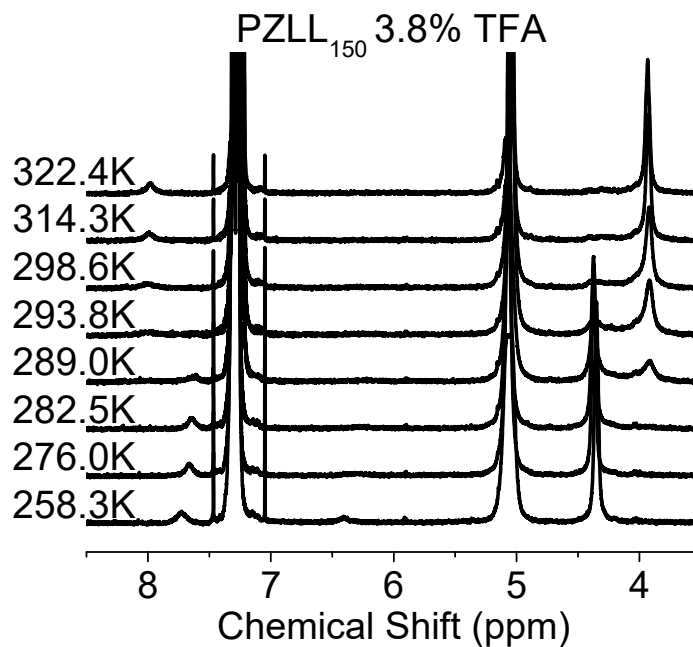


**Figure S20** <sup>1</sup>H NMR spectra of Temperature induced helix-to-coil transition of PZLL<sub>150</sub> in TFA-d/CDCl<sub>3</sub> mixture. The TFA volume concentration is 3.8%.

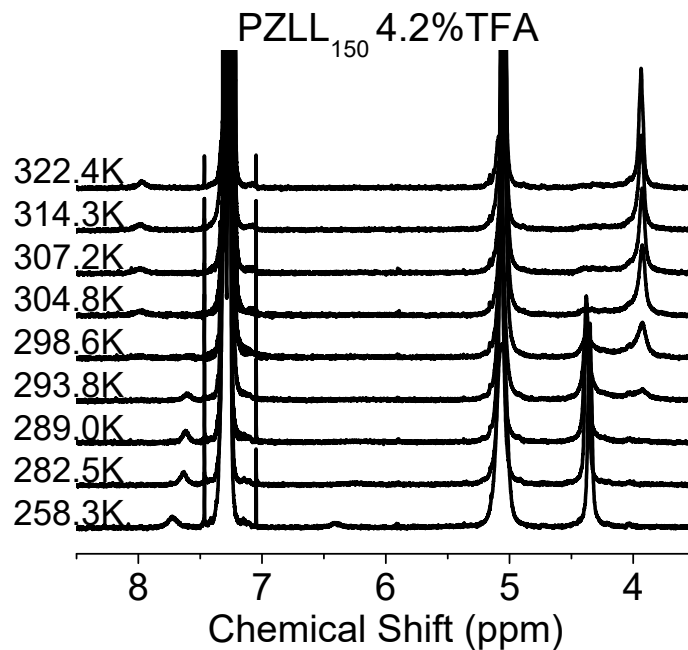


**Figure S21** <sup>1</sup>H NMR spectra of Temperature induced helix-to-coil transition of PZLL<sub>150</sub> in TFA-d/CDCl<sub>3</sub> mixture. The TFA volume concentration is 4.2%.

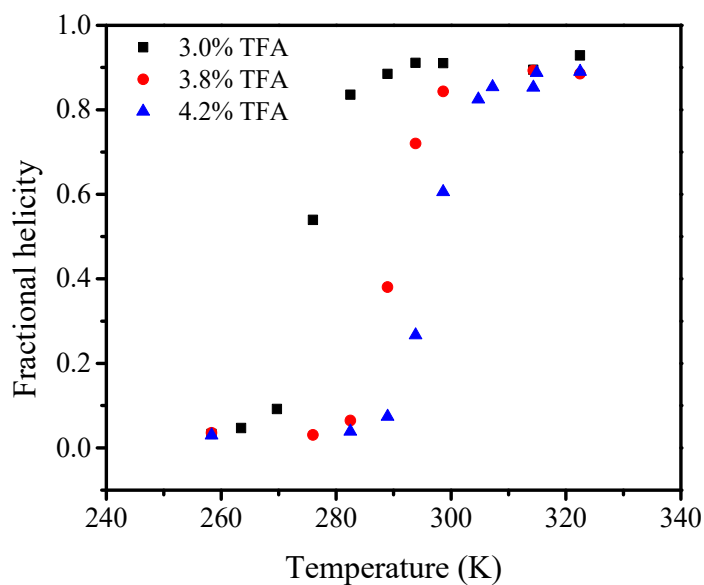


**Figure S22** Temperature induced helix-to-coil transition of PZLL<sub>150</sub> in TFA-d/CDCl<sub>3</sub> mixture.

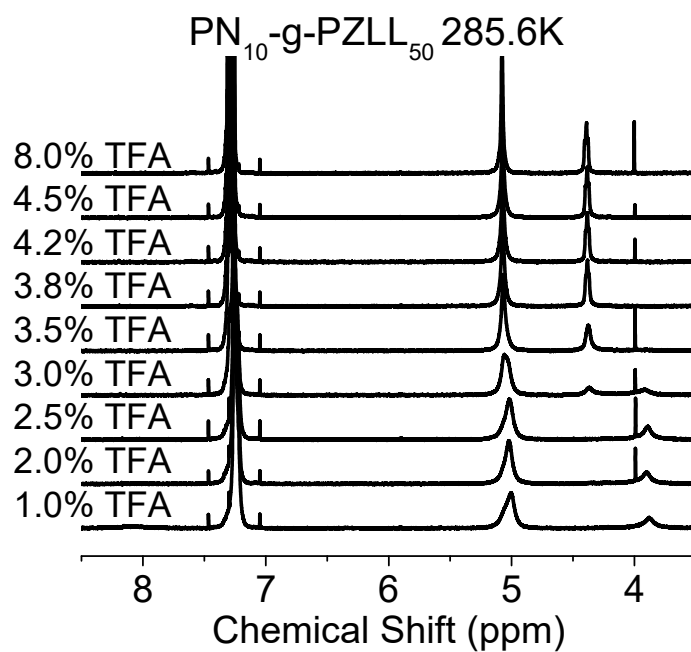


**Figure S23** TFA induced helix-to-coil transition of PN<sub>10</sub>-g-PZLL<sub>50</sub> in TFA-d/CDCl<sub>3</sub> mixture. The temperature is 285.6K

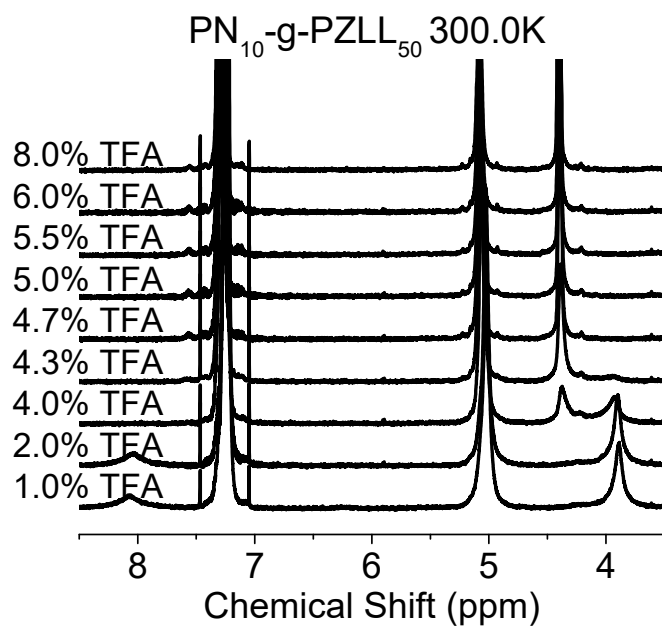


**Figure S24** TFA induced helix-to-coil transition of PN<sub>10</sub>-g-PZLL<sub>50</sub> in TFA-d/CDCl<sub>3</sub> mixture. The temperature is 300.0K

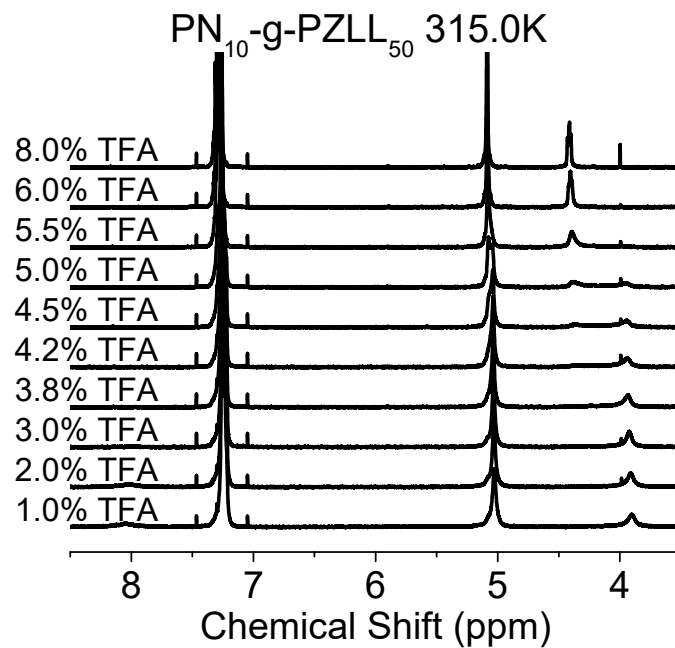


**Figure S25** TFA induced helix-to-coil transition of PN<sub>10</sub>-g-PZLL<sub>50</sub> in TFA-d/CDCl<sub>3</sub> mixture. The temperature is 315.0K.

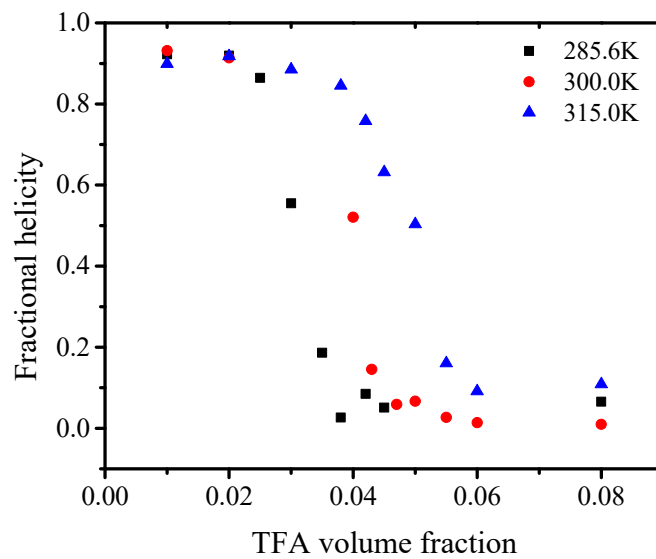


**Figure S26** TFA induced helix-to-coil transition of PN<sub>10</sub>-g-PZLL<sub>50</sub> in TFA-d/CDCl<sub>3</sub> mixture.

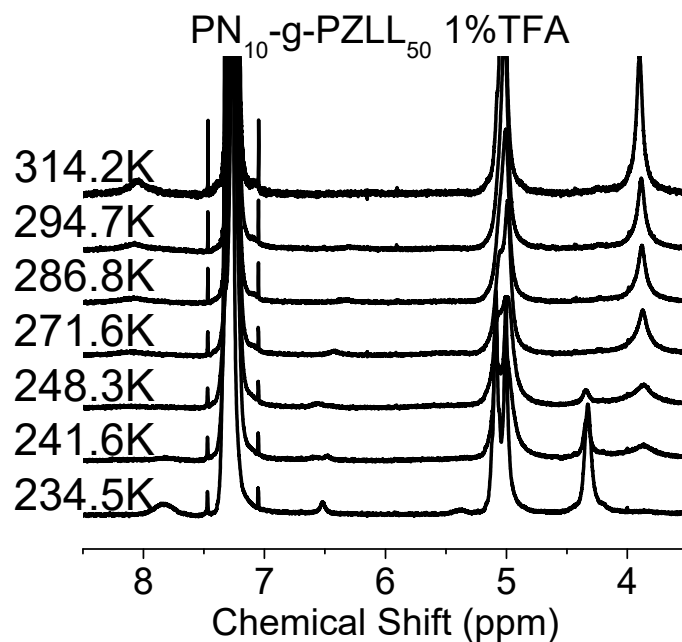


**Figure S27** Temperature induced helix-to-coil transition of PN<sub>10</sub>-g-PZLL<sub>50</sub> in TFA-d/CDCl<sub>3</sub> mixture. The TFA volume concentration is 1.0%.

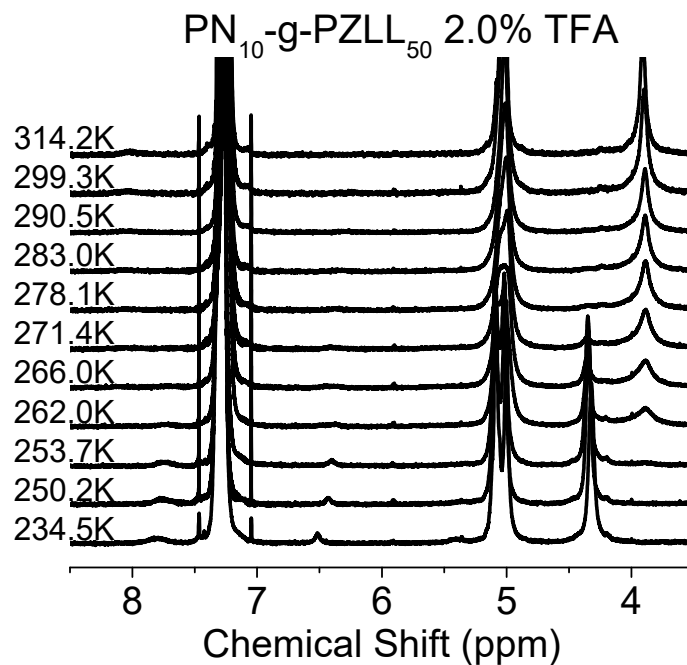


**Figure S28** Temperature induced helix-to-coil transition of PN<sub>10</sub>-g-PZLL<sub>50</sub> in TFA-d/CDCl<sub>3</sub> mixture. The TFA volume concentration is 2.0%.

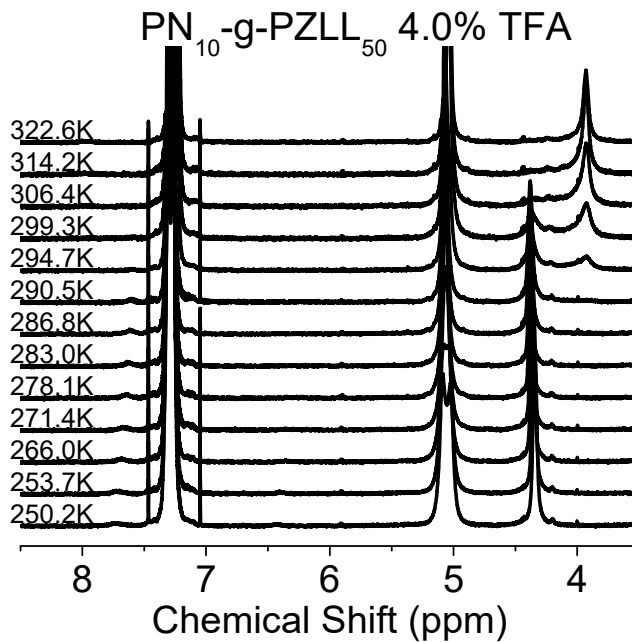


**Figure S29** Temperature induced helix-to-coil transition of PN<sub>10</sub>-g-PZLL<sub>50</sub> in TFA-d/CDCl<sub>3</sub> mixture. The TFA volume concentration is 4.0%.

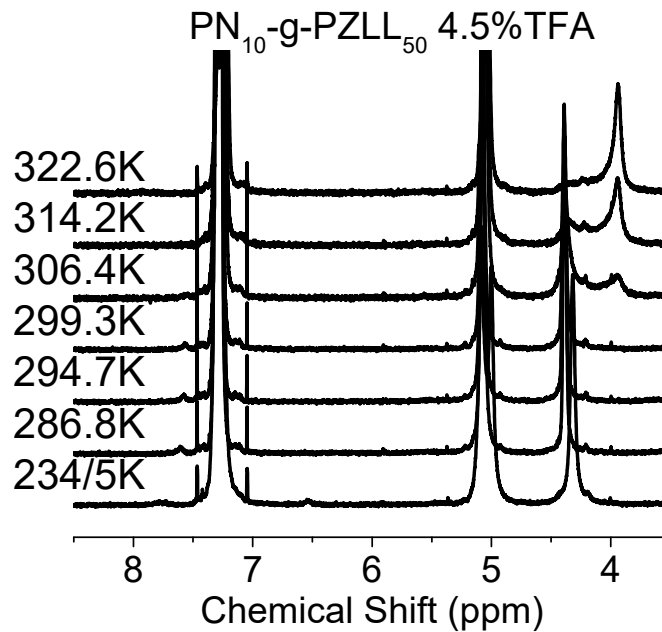


**Figure S30** Temperature induced helix-to-coil transition of PN<sub>10</sub>-g-PZLL<sub>50</sub> in TFA-d/CDCl<sub>3</sub> mixture. The TFA volume concentration is 4.5%.

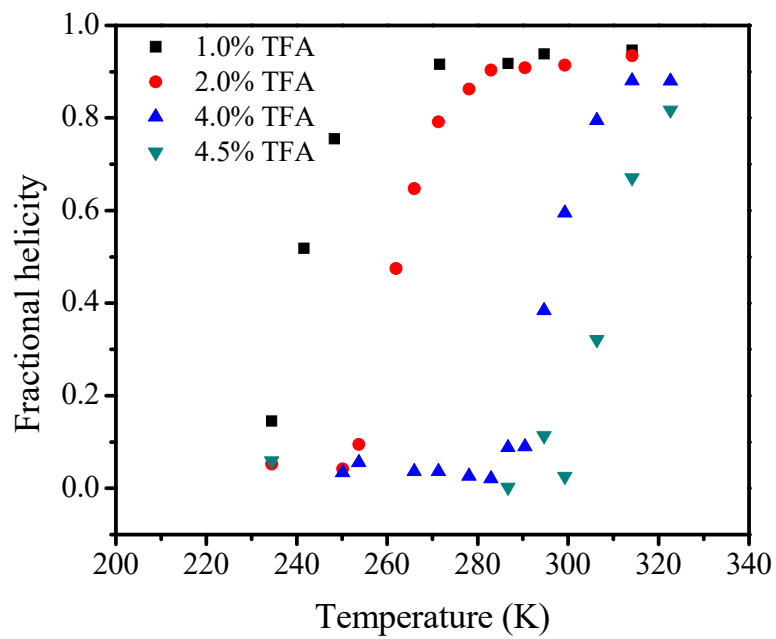


**Figure S31** Temperature induced helix-to-coil transition of PN<sub>10</sub>-g-PZLL<sub>50</sub> in TFA-d/CDCl<sub>3</sub> mixture.

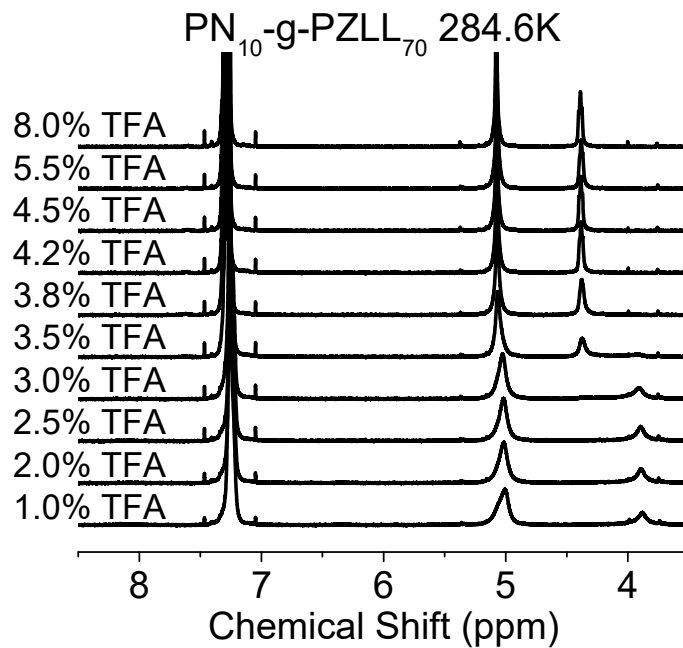


**Figure S32** TFA induced helix-to-coil transition of PN<sub>10</sub>-g-PZLL<sub>70</sub> in TFA-d/CDCl<sub>3</sub> mixture. The temperature is 284.6K.

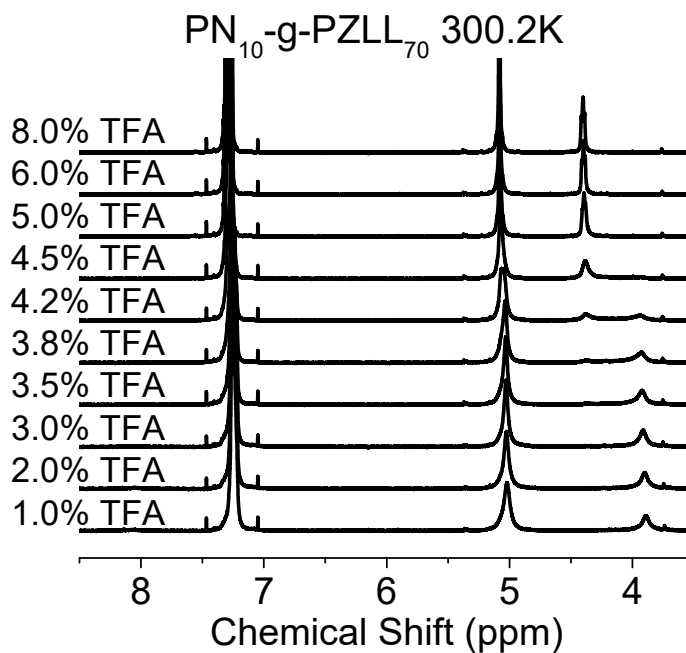


**Figure S33** TFA induced helix-to-coil transition of PN<sub>10</sub>-g-PZLL<sub>70</sub> in TFA-d/CDCl<sub>3</sub> mixture. The temperature is 300.2K.

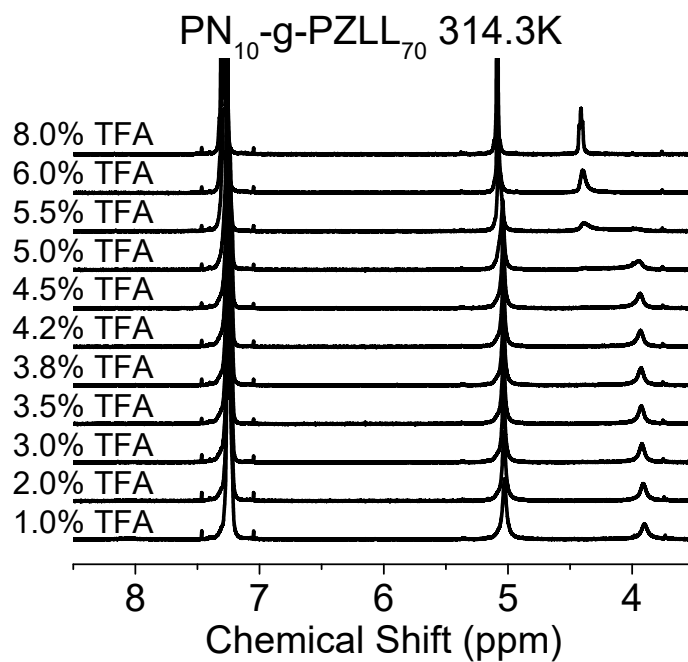


**Figure S34** TFA induced helix-to-coil transition of PN<sub>10</sub>-g-PZLL<sub>70</sub> in TFA-d/CDCl<sub>3</sub> mixture. The temperature is 314.3K.

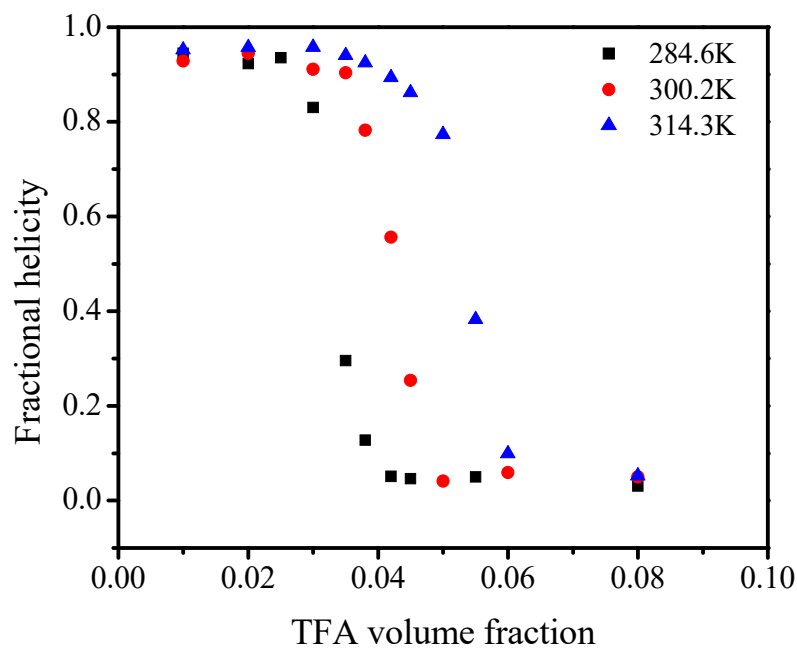


**Figure S35** TFA induced helix-to-coil transition of PN<sub>10</sub>-g-PZLL<sub>70</sub> in TFA-d/CDCl<sub>3</sub> mixture.

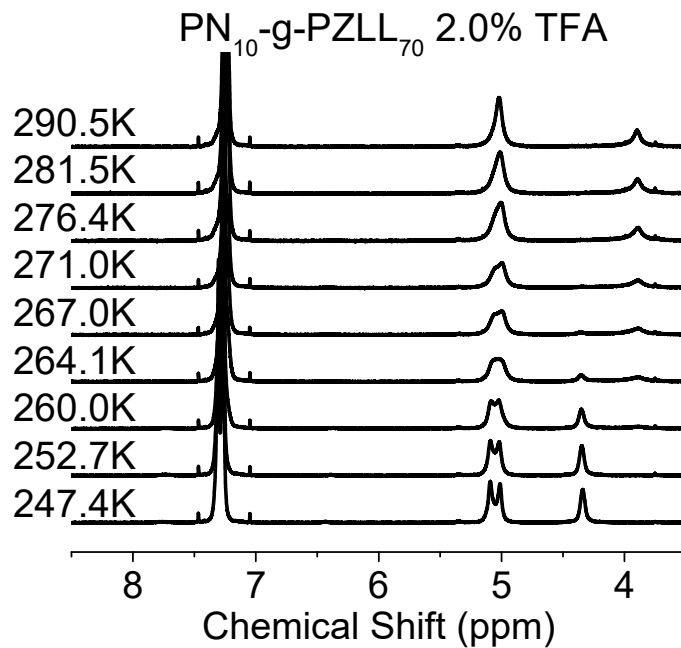


**Figure S36** Temperature induced helix-to-coil transition of PN<sub>10</sub>-g-PZLL<sub>70</sub> in TFA-d/CDCl<sub>3</sub> mixture. The TFA volume concentration is 2.0%.

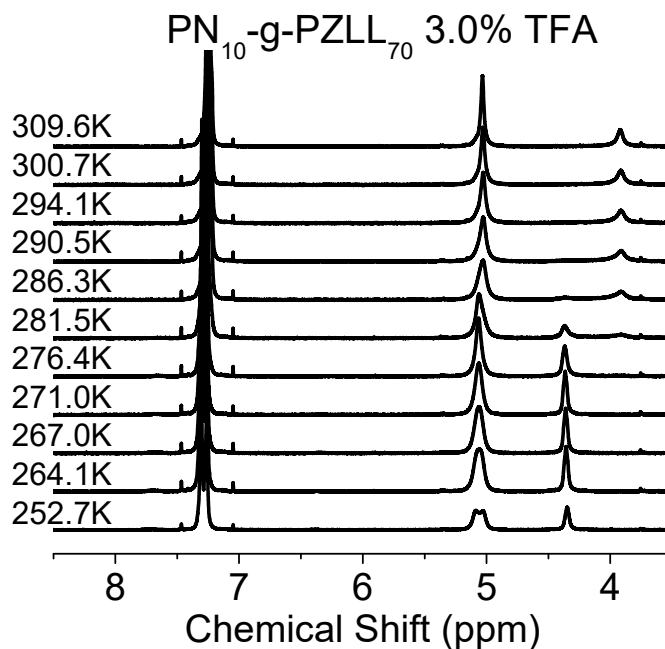


**Figure S37** Temperature induced helix-to-coil transition of PN<sub>10</sub>-g-PZLL<sub>70</sub> in TFA-d/CDCl<sub>3</sub> mixture. The TFA volume concentration is 3.0%.

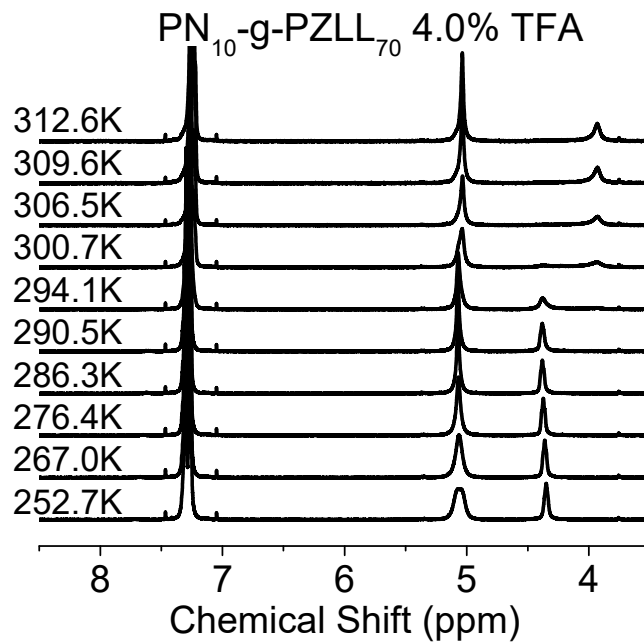


**Figure S38** Temperature induced helix-to-coil transition of PN<sub>10</sub>-g-PZLL<sub>70</sub> in TFA-d/CDCl<sub>3</sub> mixture. The TFA volume concentration is 4.0%.

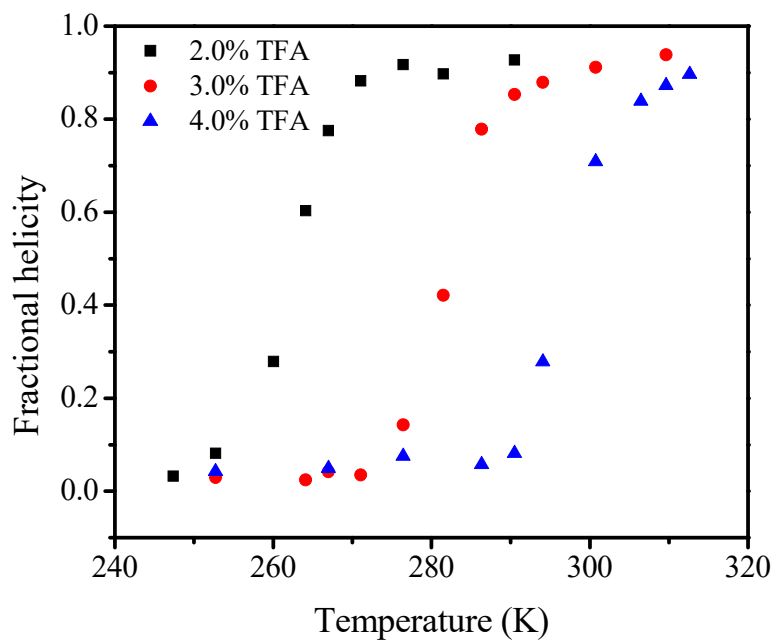


**Figure S39** Temperature induced helix-to-coil transition of PN<sub>10</sub>-g-PZLL<sub>70</sub> in TFA-d/CDCl<sub>3</sub> mixture.

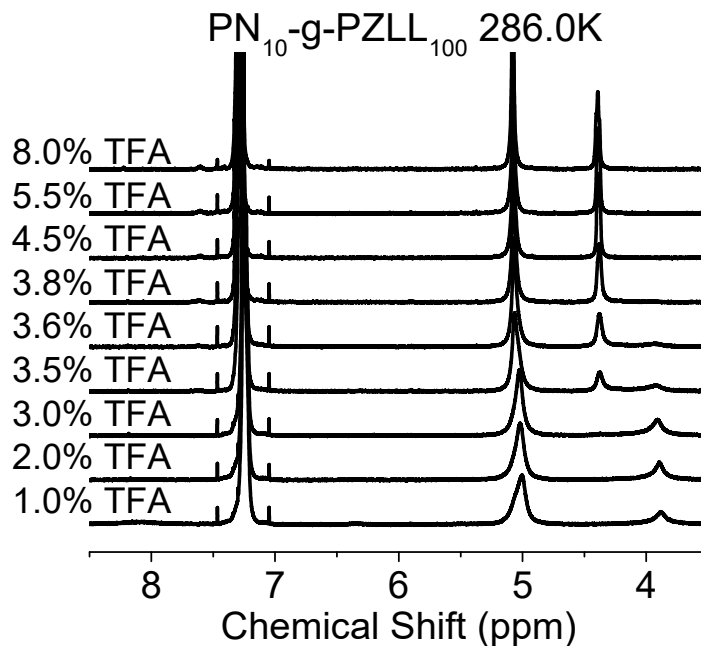


**Figure S40** TFA induced helix-to-coil transition of PN<sub>10</sub>-g-PZLL<sub>100</sub> in TFA-d/CDCl<sub>3</sub> mixture. The temperature is 286.0K.

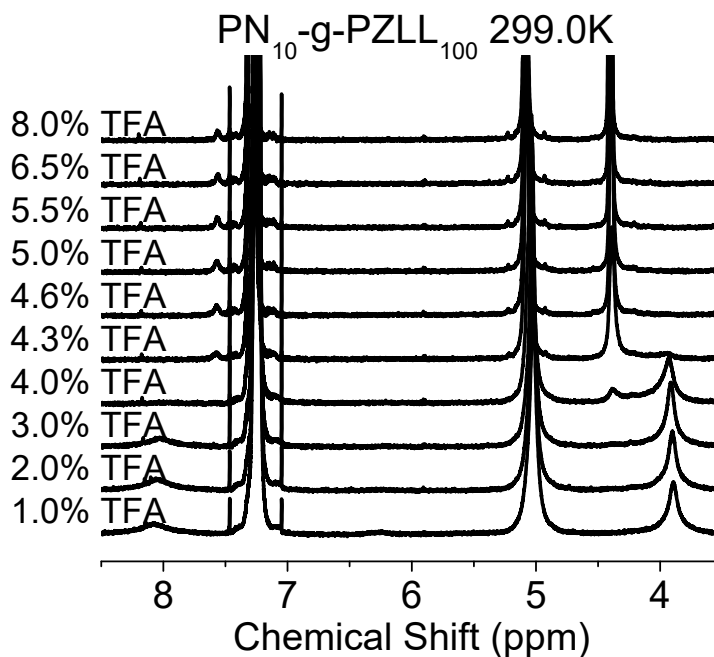


**Figure S41** TFA induced helix-to-coil transition of PN<sub>10</sub>-g-PZLL<sub>100</sub> in TFA-d/CDCl<sub>3</sub> mixture. The temperature is 299.0K.

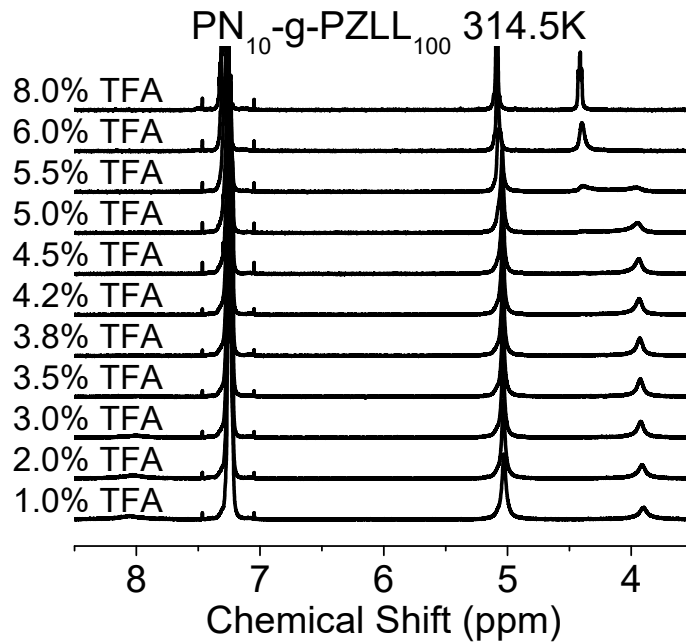


**Figure S42** TFA induced helix-to-coil transition of PN<sub>10</sub>-g-PZLL<sub>100</sub> in TFA-d/CDCl<sub>3</sub> mixture. The temperature is 314.5K.

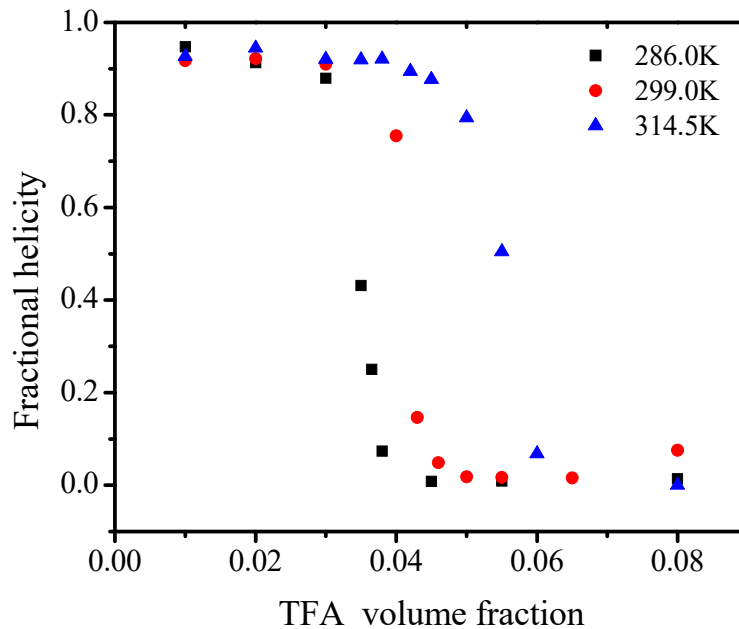


**Figure S43** TFA induced helix-to-coil transition of PN<sub>10</sub>-g-PZLL<sub>100</sub> in TFA-d/CDCl<sub>3</sub> mixture.

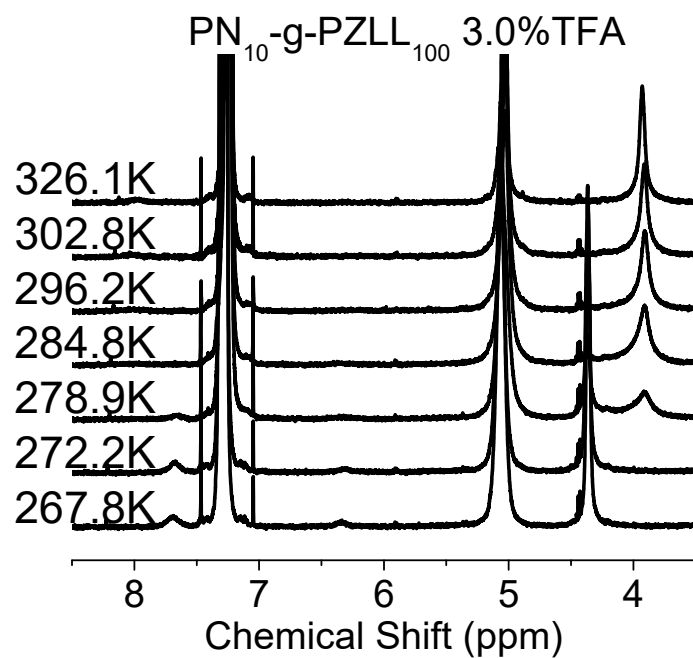


**Figure S44** Temperature induced helix-to-coil transition of PN<sub>10</sub>-g-PZLL<sub>100</sub> in TFA-d/CDCl<sub>3</sub> mixture. The TFA volume concentration is 3.0%.

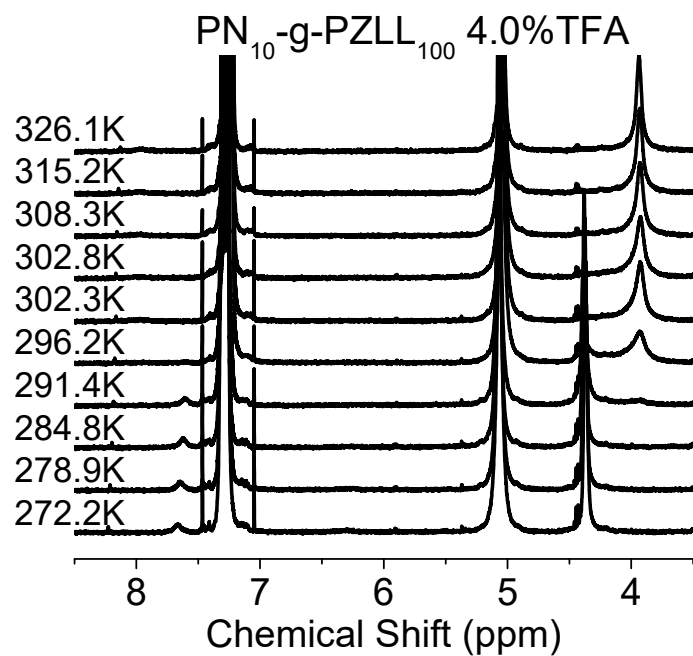


**Figure S45** Temperature induced helix-to-coil transition of PN<sub>10</sub>-g-PZLL<sub>100</sub> in TFA-d/CDCl<sub>3</sub> mixture. The TFA volume concentration is 4.0%.

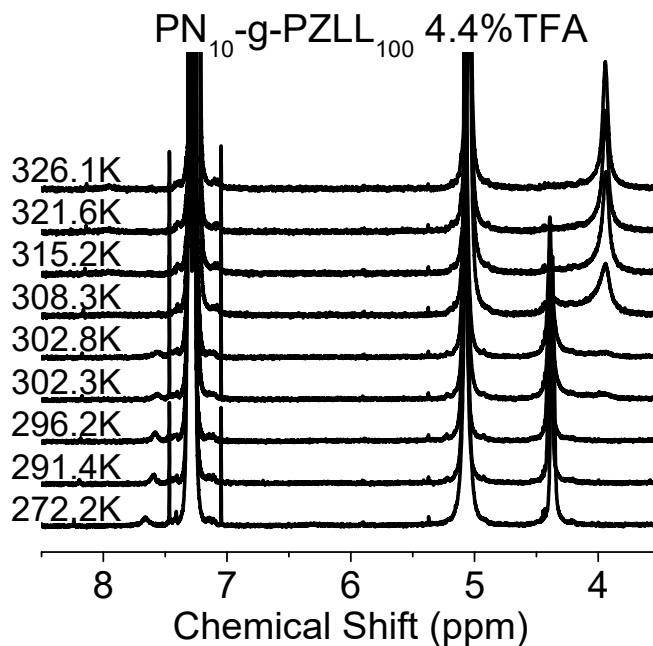


**Figure S46** Temperature induced helix-to-coil transition of  $\text{PN}_{10}\text{-g-PZLL}_{100}$  in TFA- $d_3\text{-CDCl}_3$  mixture. The TFA volume concentration is 4.4%.

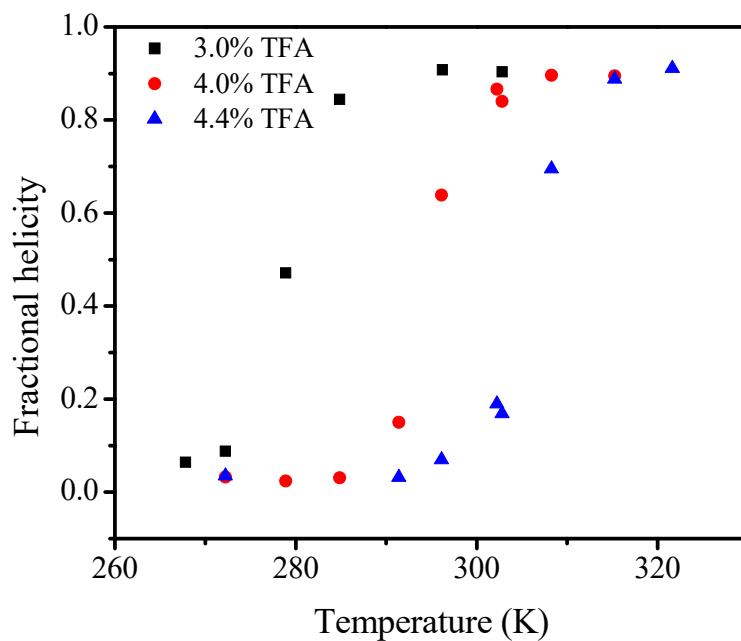


**Figure S47** Temperature induced helix-to-coil transition of  $\text{PN}_{10}\text{-g-PZLL}_{100}$  in TFA- $d_3\text{-CDCl}_3$  mixture.

Global fit of all the data using Ghosh-Dill model of TFA- and temperature-induced helix-coil transitions of linear PZLLs. (A) PZLL35, (B) PZLL63, (C) PZLL89, and (D) PZLL150 in chloroform. Filled symbols represent the experimental data; solid lines represent the global fit of all the data using Ghosh-Dill model.

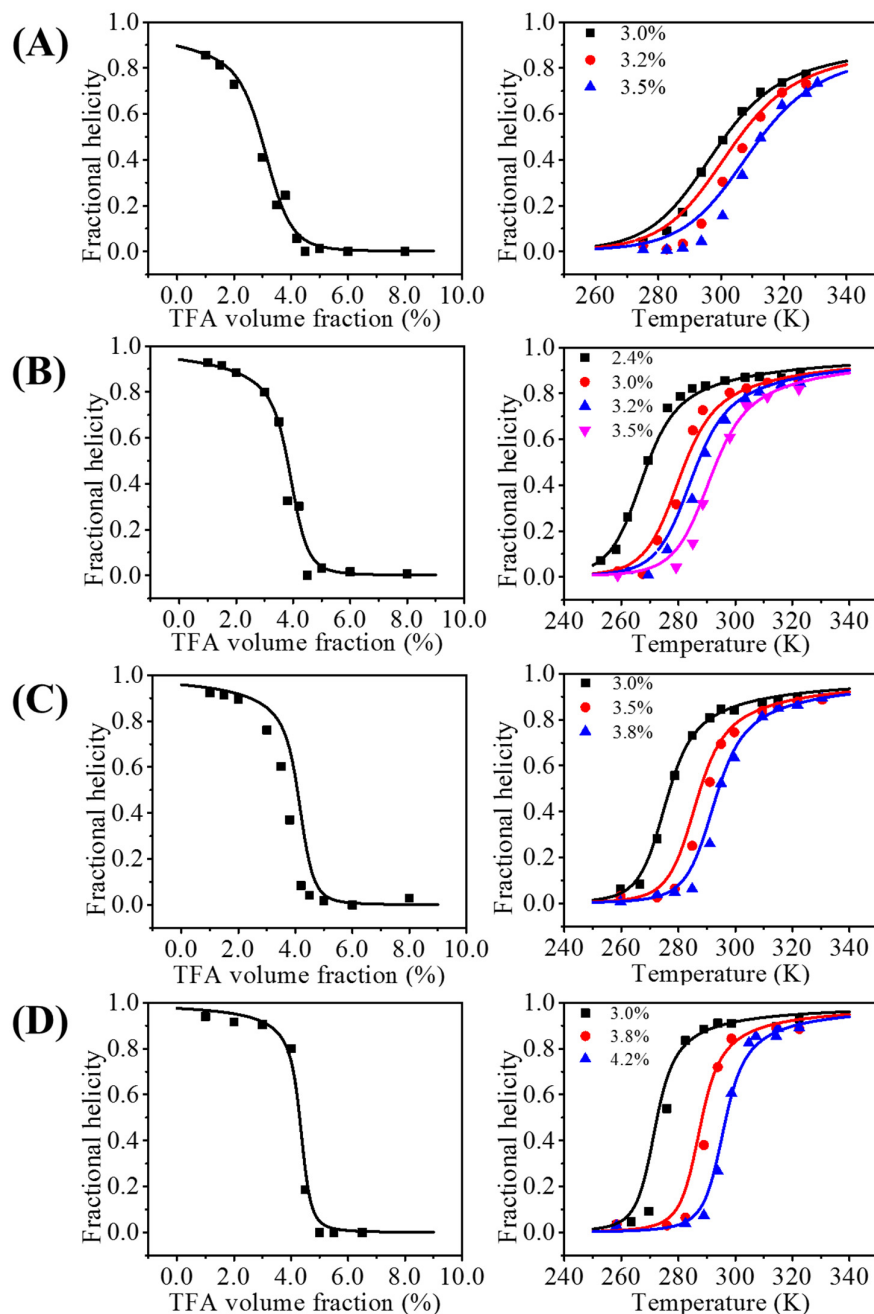


**Figure S48.** TFA- and temperature-induced helix-coil transitions of (A) PZLL35, (B) PZLL63, (C) PZLL89, and (D) PZLL150 in chloro-form globally fitted by Ghosh-Dill model.

**NOESY study of different polymers. (Figure S46-S52).** Polymers for NOESY experiments were dissolved in 98:2 CDCl<sub>3</sub>:d-TFA and sealed in NMR tubes to prevent solvent evaporation. 2D NOESY experiments were performed on a Bruker DRX-500 MHz spectrometer with the  $(\pi/2)$ - $t_1$ - $(\pi/2)$ - $\tau_m$ - $(\pi/2)$ - $t_2$  pulse sequence. 2048K spectra were acquired with a sweep width of 6510 Hz in each dimension. The  $\pi/2$  pulse width was 8.4  $\mu$ s,  $m$  was 100 ms, and the delay between acquisitions was 2 s.

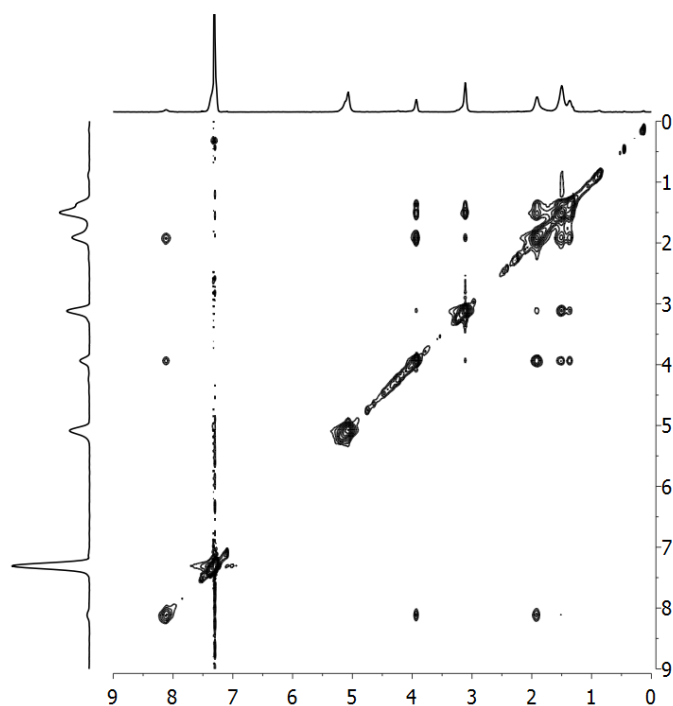


**Figure S49** The NOESY spectrum of PZLL<sub>35</sub> obtained by using the  $(\pi/2)$ - $t_1$ - $(\pi/2)$ - $\tau_m$ - $(\pi/2)$ - $t_2$  pulse sequence.

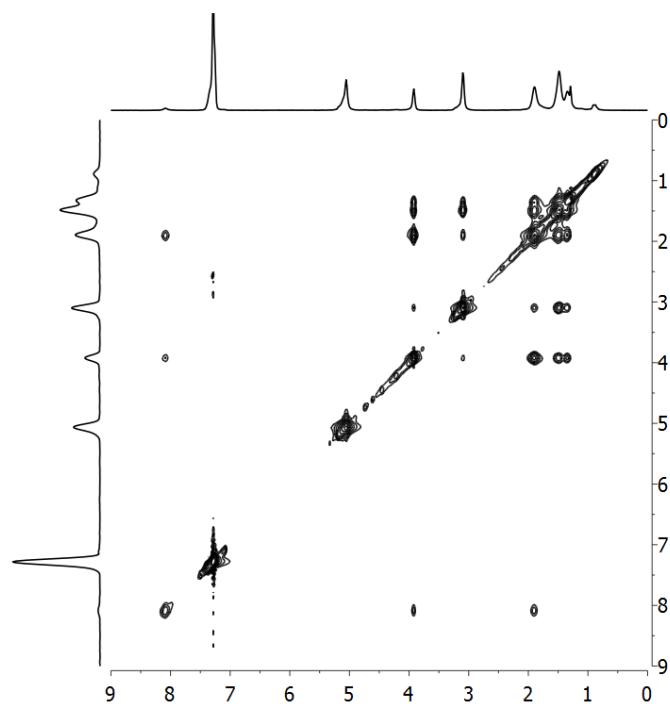


**Figure S50** The NOESY spectrum of PZLL<sub>63</sub> obtained by using the  $(\pi/2)-t_1-(\pi/2)-\tau_m - (\pi/2)-t_2$  pulse sequence.

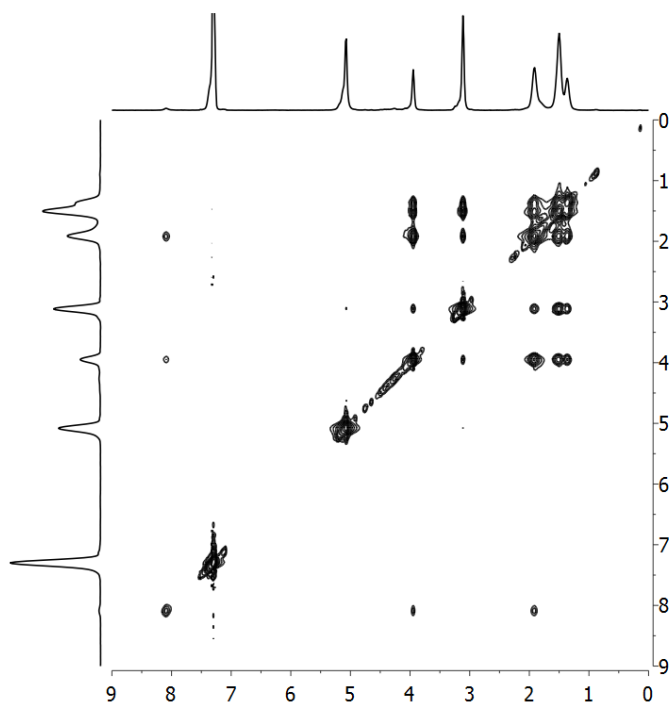


**Figure S51** The NOESY spectrum of PZLL<sub>89</sub> obtained by using the  $(\pi/2)-t_1-(\pi/2)-\tau_m - (\pi/2)-t_2$  pulse sequence.

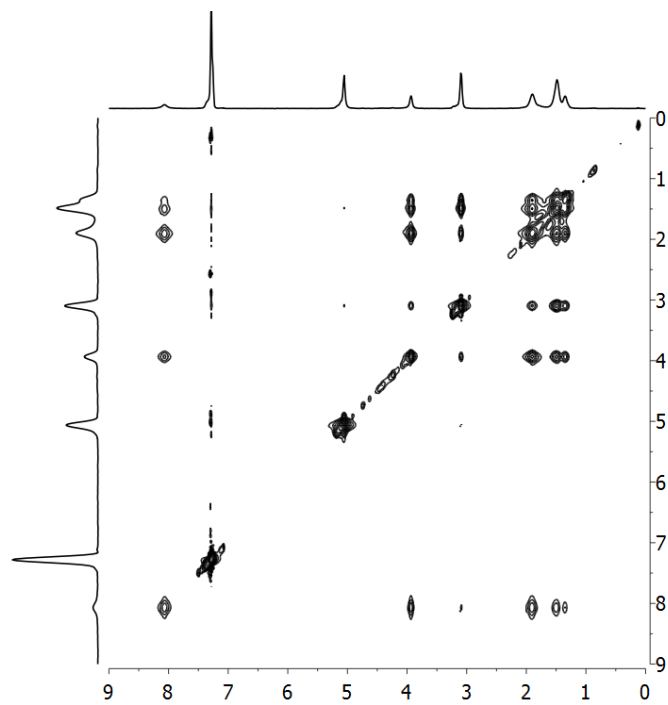


**Figure S52** The NOESY spectrum of PZLL<sub>150</sub> obtained by using the  $(\pi/2)-t_1-(\pi/2)-\tau_m-(\pi/2)-t_2$  pulse sequence.

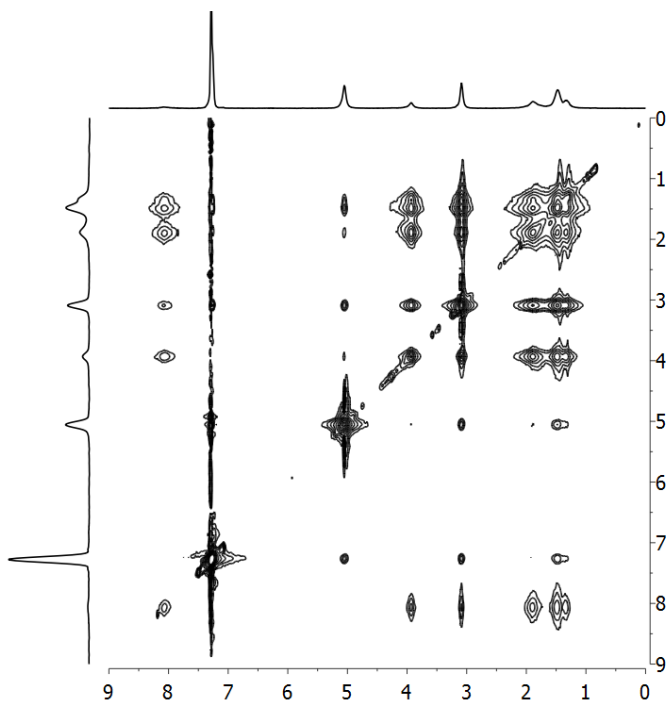


**Figure S53** The NOESY spectrum of PN<sub>10</sub>-g-PZLL<sub>50</sub> obtained by using the  $(\pi/2)-t_1-(\pi/2)-\tau_m-(\pi/2)-t_2$  pulse sequence.

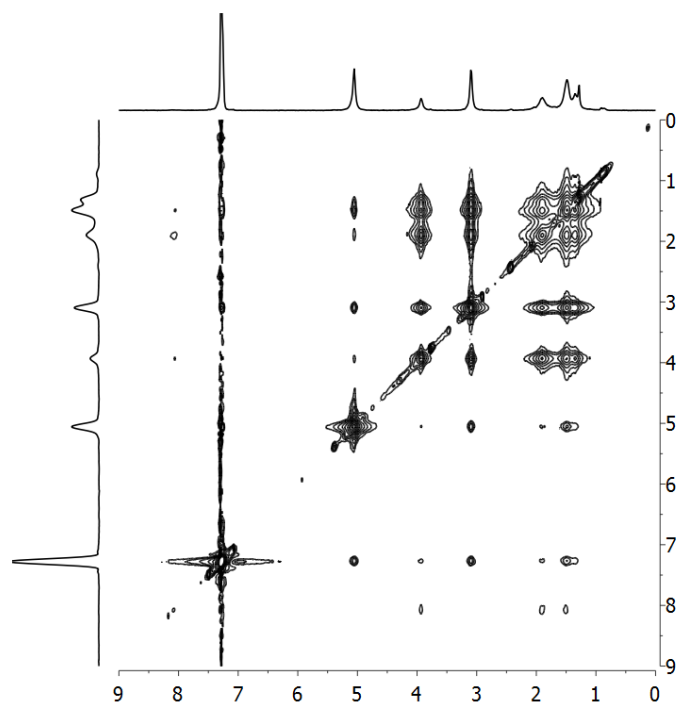


**Figure S54** The NOESY spectrum of PN<sub>10</sub>-g-PZLL<sub>70</sub> obtained by using the  $(\pi/2)$ - $t_1$ - $(\pi/2)$ - $\tau_m$ - $(\pi/2)$ - $t_2$  pulse sequence.

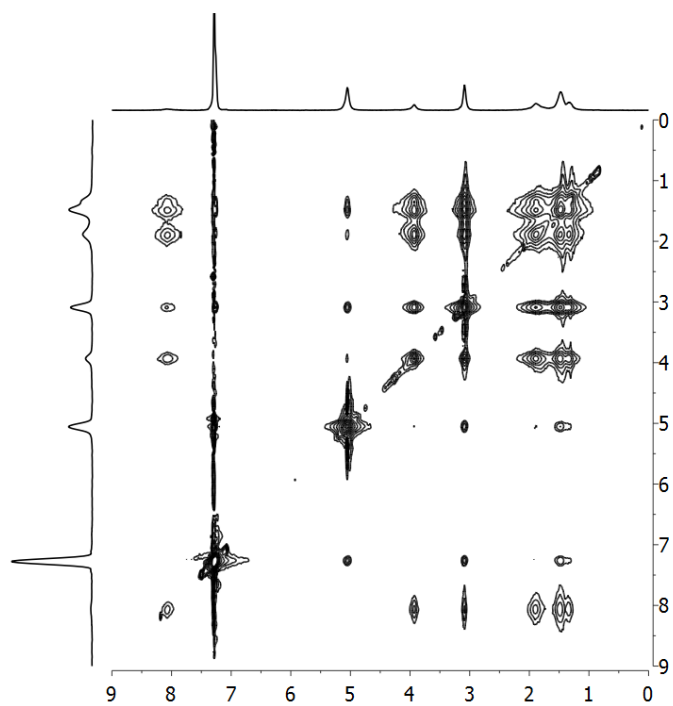


**Figure S55** The NOESY spectrum of PN<sub>10</sub>-g-PZLL<sub>100</sub> obtained by using the  $(\pi/2)$ - $t_1$ - $(\pi/2)$ - $\tau_m$ - $(\pi/2)$ - $t_2$  pulse sequence.

**Effect of variation of  $\sigma$  on the fitting of PZLL-grafted comb macromolecules.** TFA- and temperature-induced helix-coil transitions of (A) PN<sub>10</sub>-g-PZLL<sub>50</sub>, (B) PN<sub>10</sub>-g-PZLL<sub>70</sub>, and (C) PN<sub>10</sub>-g-PZLL<sub>100</sub> in chloroform. Filled symbols represent the experimental data; solid lines represent the global fit of all the data using Eq. 1, 2 and 3 with the same thermodynamic parameters ( $\Delta H^0 = 708$  cal/mol,  $\Delta S = 3.39$  cal/(K·mol), and  $m = 69.7$  cal/(mol·vol%)) obtained from linear PZLL polymers by fitting the value of  $\sigma$ . The optimized value of  $\sigma$  is  $6.91 \times 10^{-4}$ .

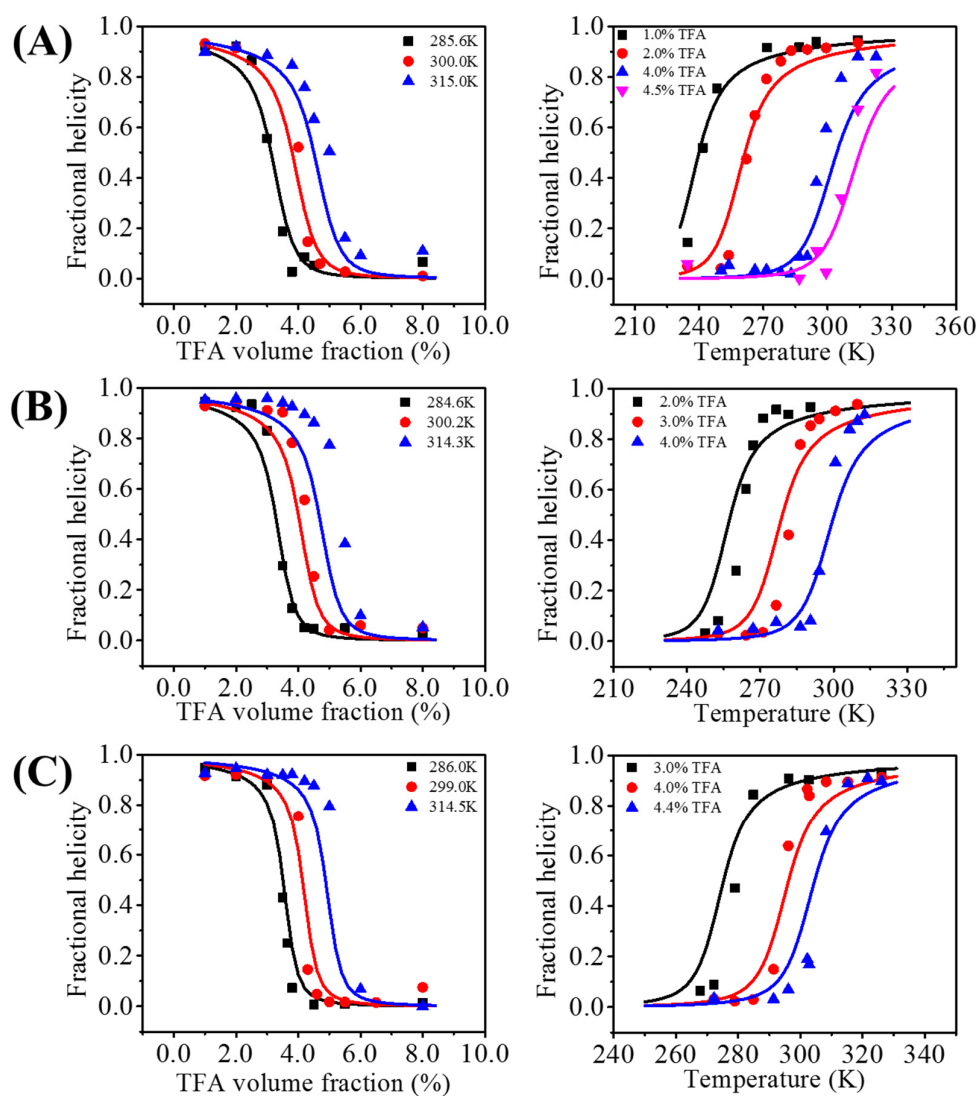


**Figure S56** TFA- and temperature-induced helix-coil transitions of (A) PN<sub>10</sub>-g-PZLL<sub>50</sub>, (B) PN<sub>10</sub>-g-PZLL<sub>70</sub>, and (C) PN<sub>10</sub>-g-PZLL<sub>100</sub> in chloroform.

**Effect of variation of chain length (N) on the fitting of PZLL-grafted comb macromolecules.** TFA- and temperature-induced helix-coil transitions of (A) PN<sub>10</sub>-g-PZLL<sub>50</sub>, (B) PN<sub>10</sub>-g-PZLL<sub>70</sub>, and (C) PN<sub>10</sub>-g-PZLL<sub>100</sub> in chloroform. Filled symbols represent the experimental data; solid lines represent the global fit of all the data using Eq. 1, 2 and 3 with the same thermodynamic parameters ( $\sigma = 2.24 \times 10^{-4}$ ,  $\Delta H^0 = 708$  cal/mol,  $\Delta S = 3.39$  cal/(K·mol), and  $m = 69.7$  cal/(mol·vol%)) obtained from linear PZLL polymers by fitting the “apparent” chain length for three samples (N = 78, 96 and 125).

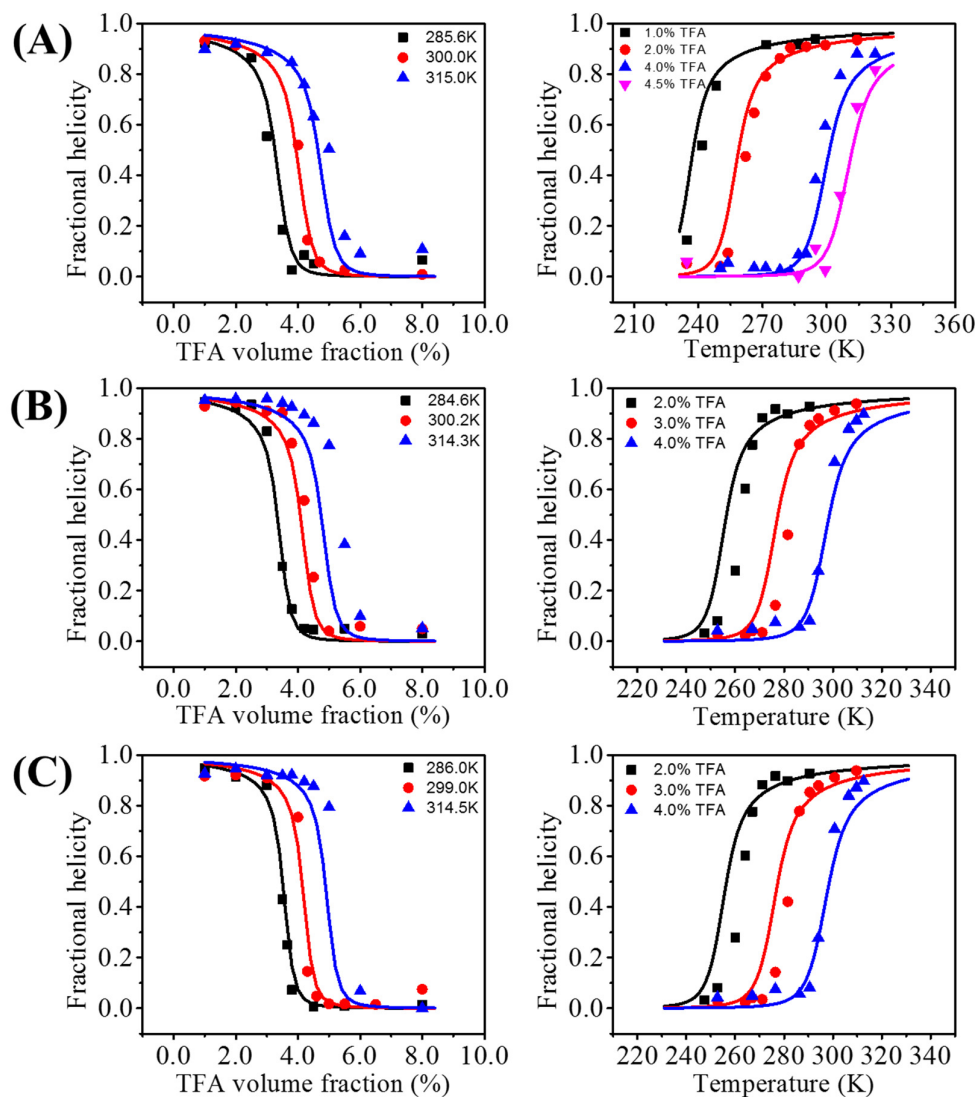


**Figure S57** TFA- and temperature-induced helix-coil transitions of (A) PN<sub>10</sub>-g-PZLL<sub>50</sub>, (B) PN<sub>10</sub>-g-PZLL<sub>70</sub>, and (C) PN<sub>10</sub>-g-PZLL<sub>100</sub> in chloroform.

Reference:

1. H. Lu and J. Cheng, "Hexamethyldisilazane-Mediated Controlled Polymerization of  $\alpha$ -Amino Acid N-Carboxyanhydrides," *Journal of the American Chemical Society*, 129, 14114-14115.
2. J. Wang, H. Lu, Y. Ren, Y. Zhang, M. Morton, J. Cheng & Y. Lin, "Interrupted helical structures of grafted-polypeptides in brush-like macromolecules," *Macromolecules*, 44, 8699–8708 (2011).
3. H. Lu, J. Wang, Y. Lin & J. Cheng, "One-pot synthesis of brush-like polymers via integrated ring-opening metathesis polymerization and polymerization of amino acids N-carboxyanhydrides," *Journal of the American Chemical Society*, 131, 13582-13593 (2009).